leti
cea tech

ANNUAL
RESEARCH REPORT
2015

TECHNOLOGIES FOR BIOLOGY AND HEALTH

Leti, technology research institute

TECHNOLOGY RESEARCH INSTITUTE

LETI AT A GLANCE

Founded in **1967**

Based in **France** (Grenoble)
with offices in **USA** (Silicon Valley)
and **Japan** (Tokyo)

350
industrial partners

1,900
researchers

Committed to innovation, Leti's teams create **differentiating solutions in miniaturization and energy-efficient technologies** for its industrial partners.

Leti is a technology research institute at CEA Tech and a recognized global leader focused on miniaturization technologies enabling energy-efficient and secure IoT. Leti delivers solid expertise throughout the entire IoT chain, from sensors to data processing and computing solutions. Leti pioneered FDSOI low power platform for IoT, M&NEMS technology for low cost multisensors solutions, CoolCube™ integration for highly connected and cost effective devices.

Leti's mission is to pioneer new technologies, enabling innovative solutions to ensure Leti's industrial partners competitiveness while creating a better future. It tackles most current global issues such as the future of industry, clean and safe energies, health and wellness, sustainable transport, information and communication technologies, space exploration and safety & security.

For 50 years, the institute has built long-term relationships with its partners: global industrial companies, SMEs and startups. It tailors innovative and differentiating solutions that strengthen their competitiveness and contribute to creating new jobs. Leti and its partners work together through bilateral projects, joint laboratories and collaborative research programs. Leti actively contributes to the creation of startups through its startup program.

Leti has signed partnerships with major research technology organizations and academic institutions. It is a member of the Carnot Institutes network*.

**Carnot Institutes network: French network of 34 institutes serving innovation in industry.*

2,670
patents in portfolio

60
startups created

€315
million budget

700
publications each year

ISO 9001
certified since 2000

TECHNOLOGIES FOR BIOLOGY AND HEALTH

Core R&D competencies for **microtechnologies for biology and healthcare** are the development, design, integration and qualification of micro- and nanotechnologies in many fields. These include detectors and actuators, imaging technologies, microfluidics, chemistry, biochemistry and electrochemistry, biology and instrumentation, including mechanics, software, information processing and electronics. Our teams have acquired expertise in developing product prototypes with a system-development perspective. Our facilities include cleanrooms dedicated to biochip packaging (230 m^2) and surface functionalization/bio probes grafting (100 m^2), biological laboratories with L2 rooms for bacteria, cells and human samples and biological characterization equipment such as PCR, cell microscopy and FACS (100 m^2). We also have a laboratory for synthetic chemistry, electrochemistry and characterization (430 m^2) and a microfluidic laboratory dedicated to technologies and system validation (300 m^2). With Clinatec, we placed our state-of-the-art technology and biology laboratories under one roof with a fully equipped preclinical facility hosting small and large animals and an integrated cutting-edge clinical platform operated by Grenoble University Hospital. This unit is optimal for conducting the first human medical-device clinical trials for safety and efficacy studies, as well as for hosting partner clinicians for the duration of their clinical research projects.

Contents

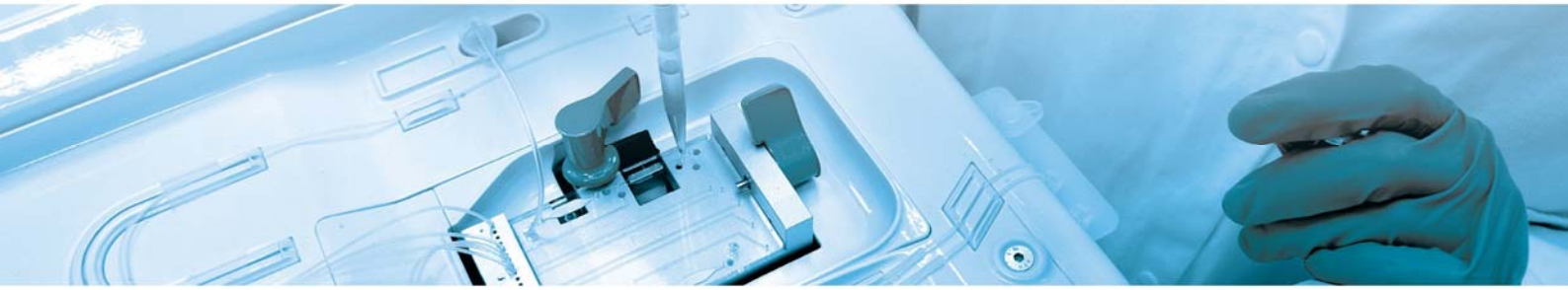

Edito

Daniel VELLOU
Head of Microtechnologies for Biology and Healthcare Division

Pr Alim Louis BENABID
Chairman of the Clinatec Board

Pr Stéphan CHABARDES
Clinatec Clinical Sector Director

"Health is a state of complete physical, mental and social wellbeing and not merely the absence of disease or infirmity." This definition from the Worldwide Health Organization when it was created in 1946 implicitly includes domains such as environment, food, wellbeing and security. Leti-Health addresses the challenges of maintaining good health, generally. Leti-Health combines 250 researchers, technicians, engineers and clinicians working in the Technology for Biology and Health Department and at Clinatec, a novel pre-clinical and clinical platform, allowing accelerated translation of the devices developed by Leti and its partners.

Together with our industrial, clinical and academic partners, we address the following application domains: *in vitro* diagnostics and monitoring for health; as well as the environment, life sciences, manufacturing and CBRN, therapeutics, nanomedicine and implanted medical devices and imaging systems for health and security. We work actively with more than 80 clinicians in Europe and worldwide in our medical device projects.

In 2015, we saw the creation of the Diabeloop start-up, which emerged from a common project between CERITD (France) and Leti. The project developed an artificial pancreas for diabetes treatment. We also have finalized regulatory testing and received authorization from clinical regulatory authorities to clinically test a Brain-Computer Interface system comprised of an implantable neural interface for long-term brain-activity monitoring and decoding, and an exoskeleton as an effector. The objective is to provide movement possibilities to motor-disabled people, in collaboration with CHU-Grenoble (France).

Our strategy is to serve industry and address societal health challenges with miniaturization and multi-modality approaches, connected devices (m-health, e-health) and deliver prototypes "ready to transfer", i.e. compliant with industry standards and medical regulations.

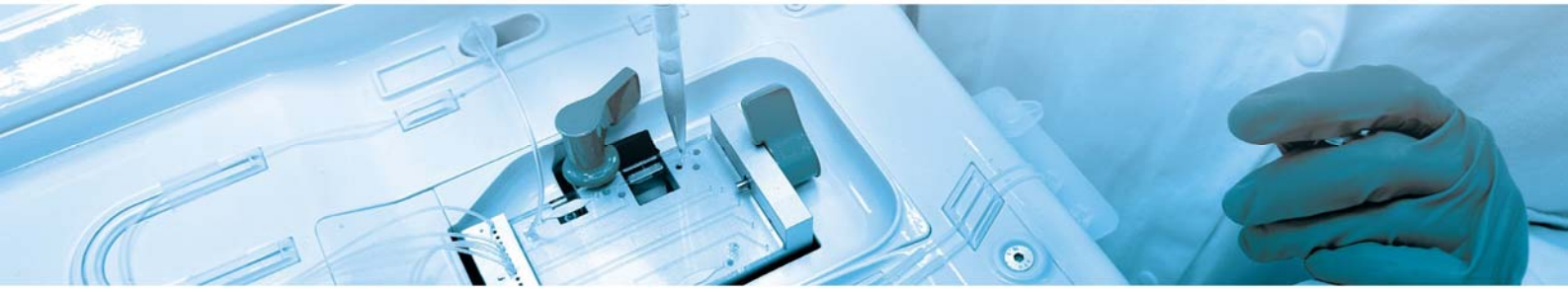

Key Figures

160 permanents researchers
95 PhDs, post-docs and short-term contracts

31 book chapters & journals
68 conferences & workshops

230 m² clean rooms for biochip packaging and surface chemistry
100 m² biological laboratory
430 m² chemical laboratory
300 m² microfluidic laboratory

6 patient rooms and a room for monitoring technologies
A fully equipped operating room with intraoperative MRI
Multimodal investigation capabilities (MEG, SPECT-CT, gait analysis)

43 patents filed in 2015
390 patents in portfolio

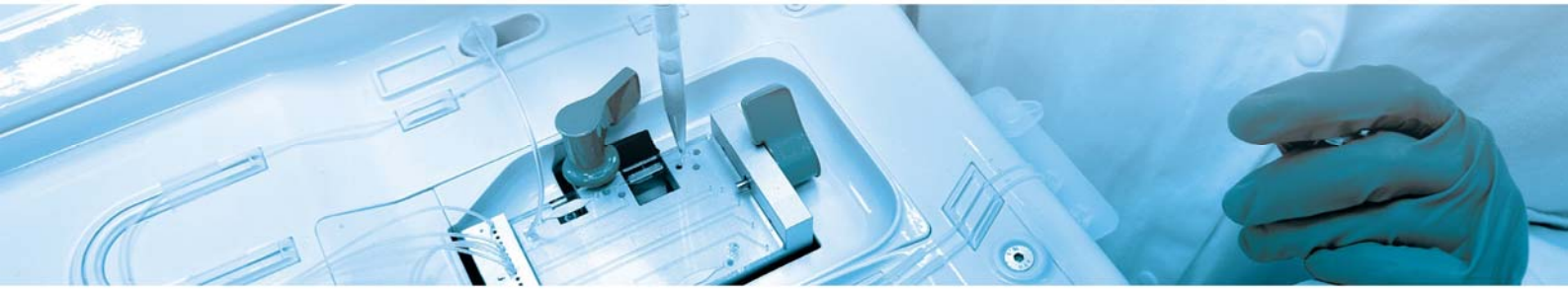

Scientific Activity

Publications

31 books chapters and journals, 68 conferences and workshops

Main papers:

Point-of-care diagnostics for ricin exposure
M. Diakite, J. Rollin, D. Jary, J. Berthier, C. Mourton-Gilles, D. Sauvaire, C. Philipp, G. Delapierre, X. Gidrol

Lab Chip. 2015 May 21;15(10):2308-17.
doi: 10.1039/c5lc00178a

WIMAGINE: wireless 64-channel ECoG recording implant for long term clinical applications
C. Mestais, G. Charvet, F. Sauter-Starace, M. Foerster, D. Ratel, AL. Benabid,

IEEE Trans Neural Syst Rehabil Eng. 2015 Jan;23(1):10-21

Prize and Awards

Guillaume Montémont received the “Best Poster Award” at ANIMMA (Advancements in Nuclear Instrumentation Measurement Methods and their Applications), 20-24 April 2015, Lisbon, for the poster **“Development and Evaluation of a Portable CZT Coded Aperture Gamma-Camera”**

Experts

5 research directors, 11 senior experts, 18 experts

Main International Collaborations

UCLA (USA), MIT (USA), LIMMS (France), Politecnico di Milano (Italy), University of Pisa (Italy), Helmotz Association (Germany), University of Twente (Netherlands), UMC Utrecht (Netherlands), SINTEF (Norway), Tyndall (Ireland), VTT (Finland), University of Liverpool (United Kingdom), CSEM (Switzerland), Charité Berlin (Germany), EMPA (Switzerland), Fraunhofer (Germany), Wake Forest University (USA), Helmholtz Association (Germany), European Technology platform for Nanomedicine (France), Max Planck Institute (Germany), Tel Aviv University (Israël), JRC-Ispra (Italy)…

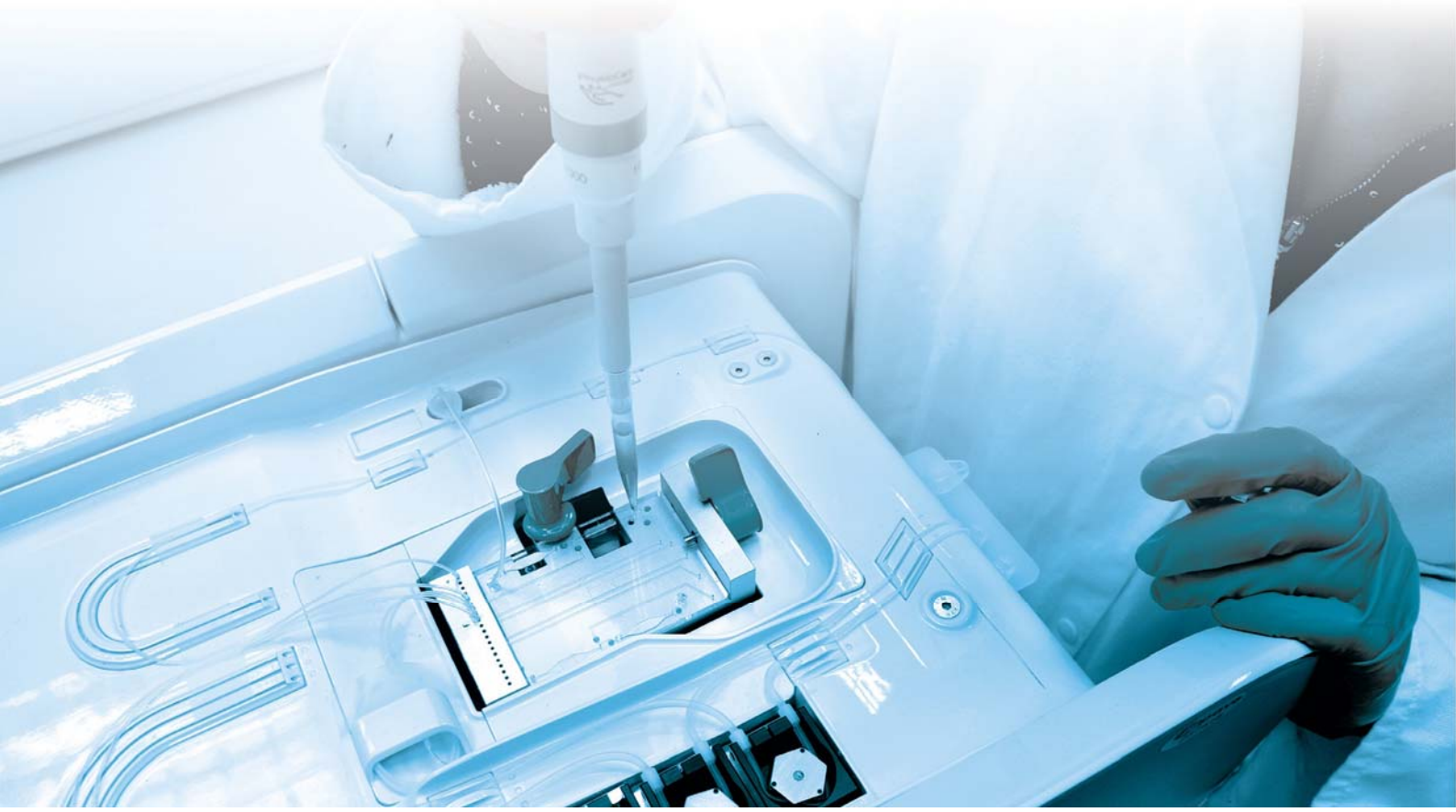

1

RADIATION DETECTION

- X-ray diffraction
- Multi energy X-ray imaging
- Gamma ray imaging
- IC for X-ray medical imaging

A novel scatter correction method for multi-energy X-ray imaging

Research topic: X-ray scattering, Multi-energy X-ray, Simulation

Authors: A. Sossin, V. Rebuffel, J. Tabary, L. Verger

Abstract: The emergence of energy-resolved photon counting detectors gives rise to new techniques in X-ray imaging. Scattered radiation induces a bias in X-ray images reducing the accuracy of such techniques. The aim of the present study was to introduce and evaluate a physical measurement based scatter correction approach adapted for multi-energy imaging. This evaluation was carried out with the aid of numerical simulations provided by an internal simulation tool, Sindbad-SFFD. A simplified thorax phantom placed in a CT geometry was used. The attenuation images and x-ray spectra visualized after correction proved to be almost scatter free.

Context and Challenges

In X-ray imaging, the signal measured in each pixel is a sum of two components: primary radiation, corresponding to photons attenuated in the inspected object, and scattered radiation, corresponding to photons scattered through Compton or Rayleigh effects. Scattered radiation induces a bias in the image giving rise to a reduction in contrast and quantification accuracy. Its presence can only be neglected for very collimated geometries. New semi-conductor based detectors [1], which can provide an energy resolved signal (spectrum) per pixel, imply an evolution of existing scatter correction methods.

Main Results

A new scatter correction method adapted for multi-energy X-ray imaging was developed [2]. It enables the estimation of the scattered radiation with the aid of a mask of attenuating elements (attenuators) inserted between the source and the inspected object. The scatter estimate is then subtracted from the original image to obtain a corrected image. The concept can be explained on two acquisitions (with and without the mask). Firstly, a subtraction of the image with mask from the image without the mask leads to a signal difference in the image zones influenced by the mask. In this signal the scatter component can be considered negligible with respect to the primary component. Then, a matrix, which describes the transition from the difference of two types of primary radiation (with and without the mask), is applied to recover the primary radiation (without mask) in the respective zones. This matrix is preliminary acquired through a calibration procedure performed experimentally or via simulations. In order to get a scattered radiation estimation, a subtraction of the recovered primary image is performed from the no-mask image. In this case, since the estimation is only obtained in sparse image zones, a regularized spatial estimation is applied on the data to recover a complete scatter image. Finally, the scatter image is subtracted from the no-mask image to obtain a corrected image. The method was evaluated on a simplified thorax phantom in a CT geometry with the aid of numerical simulations provided by an internal simulation tool Sindbad-SFFD. Attenuation images provided in Figure 1 confirm the efficacy of the proposed approach: after the application of scatter correction an increase in contrast and structure contour discernibility can be observed.

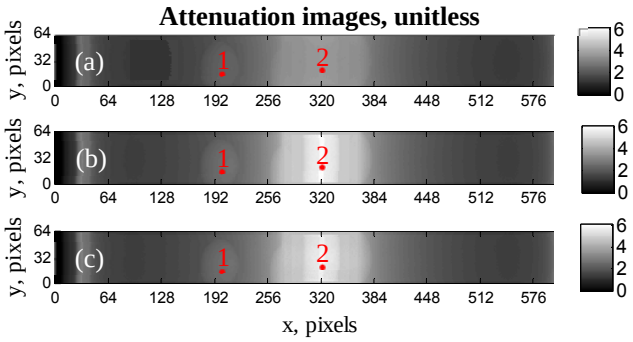

Figure 1: Total (a), primary (b) and corrected total (c) attenuation images. Control points for spectra displayed in Figure are indicated with numbers on the attenuation images.

Several spectra taken from key image pixels further confirm the accuracy of scatter correction procedure (Figure 2). The observation of Figure 2 indicates an excellent recovery of primary spectra with the scatter induced bias being almost completely reduced even for the case where the total signal in the pixel is mostly dominated by scatter (#2).

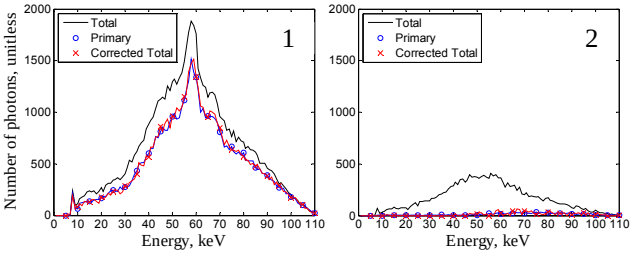

Figure 2: Total (black), primary (blue) and corrected total (red) spectra taken from control points marked in Figure 3. The spectra are sampled at equal 1 keV intervals.

Perspectives

Future studies will examine the adaptation of the method to a single acquisition protocol and corresponding attenuator mask optimization. An experimental validation of developed scatter correction approach under the double acquisition protocol is also underway.

Related Publications:
[1] A. Brambilla, P. Ouvrier-Buffet, J. Rinkel, G. Gonon, C. Boudou, and L. Verger, "CdTe Linear Pixel X-Ray Detector With Enhanced Spectrometric Performance for High Flux X-Ray Imaging", IEEE Trans. Nucl. Sci., vol. 59, no. 4, pp. 1552–1558, 2012.
[2] A. Sossin, V. Rebuffel, J. Tabary, J. M. Létang, N. Freud and L. Verger, "2015 Fast scattering simulation tool for multi-energy x-ray imaging", Nuc. Instr. and Met. in Phys. Res. A, vol. 802, pp. 60–66, 2015.

Simulation study of an X-ray diffraction system for breast cancer diagnosis

Research topic: X-ray diffraction, Imaging, Tissue analysis

Authors: F. Marticke, G. Montémont, C. Paulus, L. Verger

Abstract: X-ray diffraction (XRD) is a powerful technique used to determine the molecular structure of biological tissues. In breast tissues for example, the scattering signatures of dense fibroglandular tissue and carcinoma have been shown to be significantly different. In this study, XRD was used to perform a second level exam when conventional mammography results were unclear, for instance because of overly high breast density. A new system optimized for this issue, called multifocal XRD, was developed combining energy dispersive with angular dispersive X-ray diffraction. This system allows depth-resolved breast imaging. XRD is shown to be a very promising tool to help breast cancer diagnosis.

Context and Challenges

Conventional mammography is based on the premise that normal breast tissue and cancerous tissue differ in how they absorb X-rays. Mammography is currently believed to be the most effective breast screening tool. However, it is limited by the low contrast between the details to be detected and the background composed of adipose and fibroglandular tissues. It can lead to false negative or false positive diagnoses, resulting in missed cancer detection or unnecessary biopsies. We propose a non-invasive X-ray diffraction (XRD) method to limit the number of unnecessary biopsies. XRD can detect the molecular structure of biological tissues more specifically than X-ray absorption. In breast tissues, the scattering signatures of dense fibroglandular tissue and carcinoma have been shown to be significantly different.

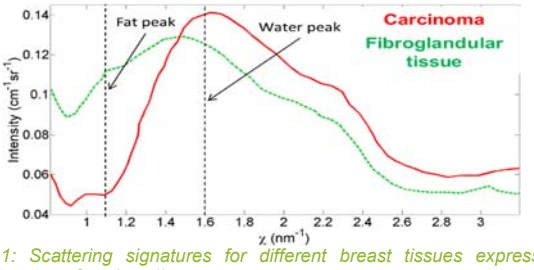

Figure 1: Scattering signatures for different breast tissues expressed in momentum transfer χ(nm-1).

Main Results

An XRD system, called multifocal XRD, was optimized for use as a second control after conventional mammography. Using a convergent collimation system and a spectroscopic imaging detector, the system combines energy dispersive XRD with angular dispersive XRD**.** This system allows depth-imaging but needs an x,y-direction scan to image the region conventional mammography identified as suspect.

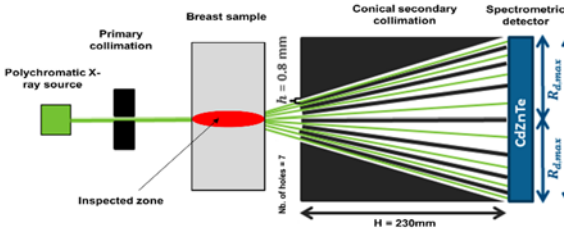

Figure 2: Optimized XRD system with multifocus collimation.

For this study, breast phantoms with and without cancerous nodule were simulated to assess the separation power of the method and to determine the radiation dose required to obtain nearly ideal separation. For tumors situated in the center of the breast, the required dose was only about 0.3mGy, even for breasts with high density. The tumor position was shown to have a low impact on detectability, provided it remained in a zone where the system was sufficiently sensitive. The influence of incident spectrum maximum energy was also studied. Although an optimum was found, the required dose remained very low with any of the incident spectra tested. Finally, an image slice was reconstructed in the x-direction and showed that the system could detect the presence of a small tumor.

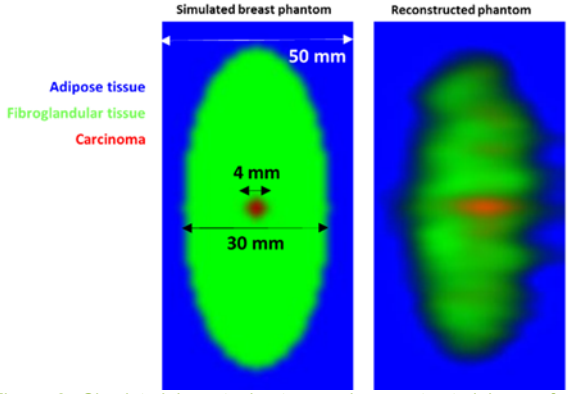

Figure 3: Simulated breast phantom and reconstructed image for incident spectra of 100 keV maximum energy with a mean dose of 0.25 mGy.

Conclusions and Perspectives

The present study indicates that coherent scattering of X-rays can be used to perform a second level exam after conventional mammography to limit the number of invasive breast biopsy. The sensitivity and specificity of the method were good even when the dose delivered was moderate. Scan-time also appears to be acceptable, with a tube current of about 10mA, scan-time for a few cm^2 was measured in seconds.

In future work, it will be necessary to manufacture the XRD system presented here so as to be able to make experimental measurements in order to confirm the simulation results. The impact of variability of tissue scattering signatures should also be studied.

Related Publications:

[1] G. Kidane, R. D. Speller, G. J. Royle, and A. M. Hanby, “X-ray scatter signatures for normal and neoplastic breast tissues”, Physics in Medicine and Biology, vol. 44, pp. 1791–1802, 1999.

[2] S. Pani, E.J. Cook, J.A. Horrocks, J.L. Jones, and R.D. Speller, “Characterization of breast tissue using energy-dispersive X-ray diffraction computed tomography”, Applied Radiation and Isotopes, 68 (10), pp. 1980-1987, 2010.

[3] B. Ghammraoui, J. Tabary, C. Paulus, V. Moulin, L. Verger, Ph. Duvauchelle, “A complete and multi purpose software tool for modeling energy dispersive X-ray diffraction”, IEEE Nuclear Science Symposium and Medical Imaging Conference, NSS/MIC 2011, Valencia.

[4] F. Marticke, C. Paulus, G. Montémont, O. Michel, J.L.Mars and L.Verger, “Multi Angle reconstruction of energy dispersive X-Ray diffraction spectra”, proc. of WHISPERS'2014, Lausanne, Suisse, 2014.

Modeling and dimensioning a novel tissue-specific breast imaging system using spectral X-ray coherent scattering

Research topic: X-ray diffusion, Imaging, Material analysis

Authors: D. Barbes, J. Tabary, C. Paulus, L. Verger

Abstract: Mammography is currently one of the most demanding imaging techniques due to a persistent difficulty to detect small microcalcifications and distinguish masses, benign or malign, from fibro-glandular tissue. This latter issue seems to be solvable with the aid of X-ray coherent scattering. For that we chose to use a specific technique of scattering measurement called Energy-Dispersive X-Ray Diffraction (EDXRD), or spectral x-ray coherent scattering which combines the use of an X-ray tube and a spectrometric detector. Therefore, this study presents the modeling of an EDXRD device as a way to identify and image biological tissues for breast cancer diagnosis.

Context and Challenges

In the field of breast imaging, the classical mammography sometimes fails at determining the cancer presence and the additional exams, like MRI or biopsy, remain either expensive or very invasive.

Some previous work showed that coherent X-ray scattering experiment provides useful information for the characterization of tissues, especially in breast cancer diagnosis [1, 2]. In this paper, we present the modeling of a device utilizing coherent scattering radiation measurement aimed to identify and image materials for a medical application.

Main Results

Our modeling tool is based on an Energy-Dispersive X-Ray Diffraction (EDXRD) system. The scattering signature of the studied object depends on a variable, called momentum transfer, combining photon energy and scattering angle. With this type of system, the signature measuring is made by recording the scattering intensity while varying the photon energy, by using a polychromatic spectrum and a spectral detector, at fixed scattering angle. This tool includes the modeling of the incident spectrum, the object attenuation and signature, the collimation response and the detector response. The combination of these elements allows us to get the spectrum measured by any pixel of the energy-resolved detector with a given configuration. The measured spectrum is then processed to get the scattering signature at any position in the studied object. These signatures are then recognized which leads to a material-specific image of the object. An example of a modeled system, based on a specific "folder-shaped" second collimation, is presented in Figure 1.

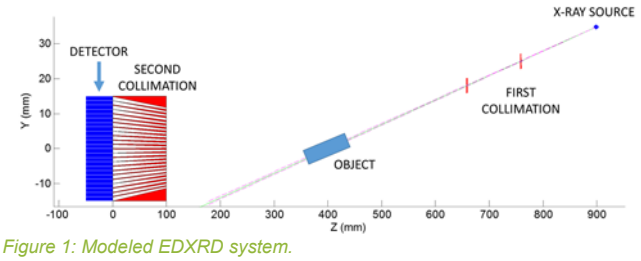

Figure 1: Modeled EDXRD system.

We modeled an existent multi-pixels CdZnTe detector conceived in our lab [3] (8x24 pixels of 2.5x1.25 mm²) and for which we assume the use of a subpixelation technique to subdivide the pixels in 4 in the Y direction. This subpixelation, which is possible by exploiting the signals induced in the neighboring anodes [4], is very useful to improve the separation of tissues in the depth of the inspected part. This configuration has been chosen for two reasons: firstly its ability to see different zones in the Z direction (see Figure 1) in one measurement, secondly to get an angle range compatible with the incident spectrum in order to scan the momentum transfer range useful for breast imaging purpose (typically from 0.5 to 2.5 nm^{-1}).

The chosen object, presented in Figure 2(a), mimics a breast sample by using three simulated materials with Gaussian signatures, centered on 1.1, 1.6 and 2.2 nm^{-1}. The first value is the position of the main peak of adipose tissue. The two others represents water and fibrous tissues [5].

Finally, Figure 2(b) represents the spatial probability coefficients for each of the three materials, returned by the identification process. Figure 2(c) shows the obtained specific image of the object, with materials of higher probability for each pixel.

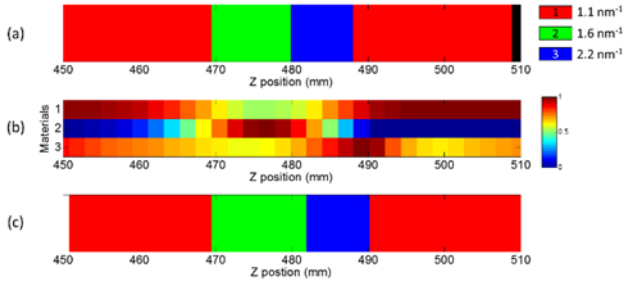

Figure 2: Object and results.

Perspectives

This study presents a modeling software aimed as a dimensioning tool to optimize the architecture of an innovative breast imaging system using spectral coherent scattering. The first results seem promising and open the way for further work. Our next task will be to use this device to design a system viable for medical use, namely in terms of dose, spatial resolution and tissue specificity. The performance of the processing can also be enhanced by the improvement of the current algorithms or the introduction of new ones.

Related Publications

[1] G. Kidane, R. D. Speller, G. J. Royle, and A. M. Hanby, 1999, "X-Ray Scatter Signatures for Normal and Neoplastic Breast Tissues", Physics in Medicine and Biology 44 (7).

[2] S. Pani, E.J. Cook, J.A. Horrocks, J.L. Jones, and R.D. Speller. 2010. "Characterization of Breast Tissue Using Energy-Dispersive X-Ray Diffraction Computed Tomography", Applied Radiation and Isotopes 68 (10): 1980–87. doi:10.1016/j.apradiso.2010.04.027.

[3] G. Montémont, D. Kosciesza, O. Monnet, S. Stanchina, J.-P. Schlomka, and L. Verger, 2013, "An Autonomous CZT Module for X-Ray Diffraction Imaging", In 2013 IEEE Nuclear Science Symposium and Medical Imaging Conference (NSS/MIC), 1–4. doi:10.1109/NSSMIC.2013.6829819.

[4] G. Montémont, S. Lux, O. Monnet, S. Stanchina, and L. Verger, 2012, "Evaluation of a CZT Gamma-Ray Detection Module Concept for SPECT", In 2012 IEEE Nuclear Science Symposium and Medical Imaging Conference (NSS/MIC), 4091–97.

[5] E.A. Ryan and M.J. Farquharson, 2007, "Breast Tissue Classification Using X-Ray Scattering Measurements and Multivariate Data Analysis", Physics in Medicine and Biology 52 (22): 6679–96.

Methods for tissue and iodine quantification in spectral mammography

Research topic: Spectral imaging, Mammography, Material decomposition

Authors: Y. Pavia, A. Brambilla, V. Rebuffel, L. Verger

Abstract: Breast density has become an important parameter to follow up during mammography exams to estimate a breast cancer risk. Until now, this measurement was performed with segmentation methods on grey-scale images or, more recently, on dual-energy acquisitions to improve the density estimation using material decomposition methods. In the meantime, contrast enhanced mammography was also developing to highlight more vascularized areas like around cancerous tissues but this technique requires double energy X-ray exposure. The emergence of energy resolved detectors will allow us to accurately estimate the breast density and vascularization in a single shot image acquisition.

Context and Challenges

Breast density is defined as a percentage of glandular tissue over the whole breast. Current techniques for its estimation are mainly based on grey-scale 2D images and miss information along the third dimension (ratio of areas). Material decomposition methods, based on measurement at different energies can overcome this limitation. Our study evaluate the performance of two material decomposition approaches: a well-known method based on polynomials usually used for two materials, extended to three for iodine quantification; and a recently developed maximum log-likelihood approach that is easily generalizable.

Main Results

We designed a specific tool for spectral mammography simulation purpose and modeled a 60 µm pixel pitch CdTe detector in a scanning slit geometry, including a charge-sharing correction, and assumed no pile-up for our simulation case. We simulated a 49 kVp tungsten spectrum that is above the iodine K-edge used as contrast agent. A 45 mm thick breast phantom, with iodine inserts, was designed using water and polymethyl-methacrylate (PMMA) to respectively mimic glandular and adipose tissues. Thus, we need to quantify these two materials to determine the breast density. Standard polynomial method for breast density quantification was initially developed with dual energy acquisition procedures (low and high energies). We extended these functions (2nd and 3rd orders) to make them compliant with 3 energy bins.
Maximum log-likelihood material decomposition was performed with 3 and 8 energy bins. Nevertheless, this approach requires an interpolation of the calibration database to allow an accurate decomposition. Cubic splines gave satisfying spectra interpolations.

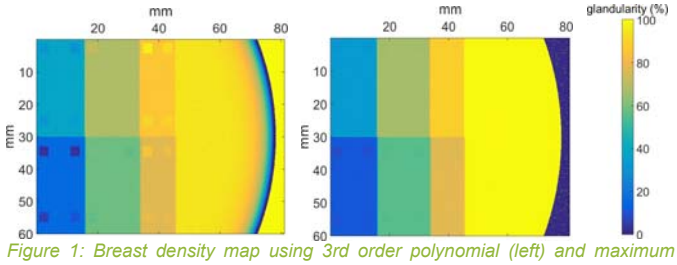

Figure 1: Breast density map using 3rd order polynomial (left) and maximum likelihood method (right).

Figure 1 shows that polynomial methods are sensitive to iodine thicknesses for breast density quantification, leading to a bias up to 10% in some areas depending on iodine thickness. In the same configuration, we noticed a maximal bias of 3.6% using the maximum likelihood method and less than 1.3% with 8 energy bins.

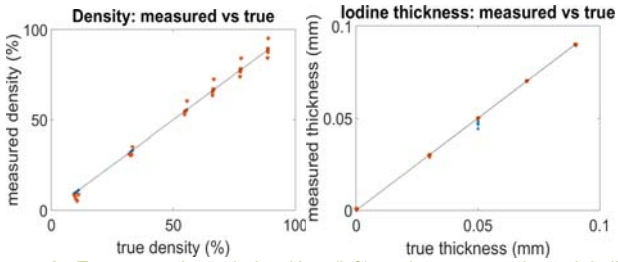

Figure 2: True vs estimated densities (left) and true vs estimated iodine thicknesses (right). Orange markers for polynomial method and blue markers for likelihood method and dark line for measured=true.

Figure 2 shows that the likelihood method clearly decreases the standard deviation (dispersion of measurements) on density by a factor of 2 compared to polynomial methods. However, polynomials are reliable for iodine quantification while likelihood approach is limited by the dataset interpolation step. A thinner interpolation step can be used to go over this limitation but will result in a higher computing time during the material decomposition process. Finally, we have shown that polynomial methods can give fast results for breast density and iodine quantification. Nevertheless, this approach is limited to a small number of energy channels on spectrometric detectors, due to large condition numbers during model inversion, and lead slightly biased results. To go further, the maximum likelihood approach achieves better results in terms of bias and noise and is less sensitive to iodine thickness variation. Moreover, this technique is easily generalizable to detectors with many energy bins.

Perspectives

This study showed the feasibility a breast density and iodine quantification using a single X-ray exposure and energy sensitive detectors, during a mammography screening exam. These results will now be experimentally validated and the maximum log-likelihood method is undergoing improvements to achieve even more accurate quantification.

Related Publications:
[1] Y. Pavia, A. Brambilla, V. Rebuffel, J.-M. Létang, N. Freud and L. Verger, “Methods for Tissue and Iodine Quantification in Spectral Mammography”, IEEE Nuclear Science Symposium and Medical Imaging Conference (NSS/MIC), San Diego, 2015.

A material base decomposition algorithm for high resolution spectroscopic X-ray imaging detectors

Research topic: X-ray imaging, Spectral imaging, Material decomposition,

Authors: A. Brambilla, A. Gorecki, A. Potop, C. Paulus, G. Gonon, V. Rebuffel, V. Moulin, L. Verger

Abstract: We have developed a material base decomposition algorithm for photon counting detectors (PCD). The method computes two images representing the equivalent lengths of the base materials from the measured attenuations corrupted by non-linear effects of the measure, such as charge sharing or pile-up. The resulting images behave linearly and provide quantitative information on the average chemical composition of the analysed samples. We used this method to measure the effective atomic number of different plastic materials with accuracy or to estimate the bone mineral density.

Context and Challenges

Energy sensitive photon counting detectors (PCDs) provide energy dependent information which can be exploited for material identification. The attenuation of an X-ray beam as a function of energy depends on the effective atomic number Z_{eff} and the electron density. However, the attenuated spectra are degraded by the imperfections of the detector response such as charge sharing or pile-up, which leads to nonlinearities in the measured attenuation functions.

This work aims to implement a basis material decomposition method which overcomes this problem. It consists in finding a combination of thicknesses from chosen basis materials that reproduces exactly the attenuation of the analysed object. The attenuated spectra are compared to those of a calibration base using a maximum likelihood criterion assuming a Poisson law distribution of count for each energy bin.

Main Results

We acquired images from different plastic materials with a ME100 linear array detector providing spectral images over 64 energy bins [1]. Figure 1 represent a PE (Z_{eff} = 5.53) cube with POM (Z_{eff} = 7.03), PVDF (Z_{eff} = 7.97) and PVC (Z_{eff} = 14.26) inserts. The acquired spectral images were decomposed on a PE/PVC base. The represented equivalent lengths depend on the Z_{eff} and density of the plastic material.

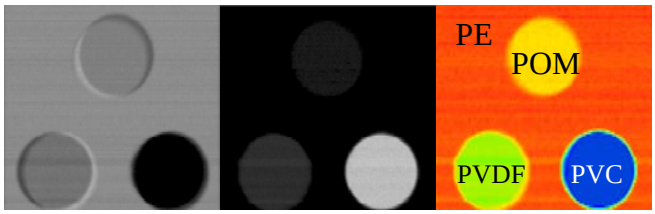

Figure 1: Images of PE (left) and PVC (middle) equivalent lengths of a test object made of PVC (thickness = 22 mm) PVDF (34 mm) and POM (42 mm) cylinders lodged in a 60x60x60 mm³ PE cube. The right image represents the Z_{eff} image deduced from the PE-PVC decomposition

The effective atomic number can be deduced from the equivalent lengths. Our approach was to decompose the theoretical spectra from simple elements ranging from carbon to aluminium. We have derived a function to convert the ratio of equivalent lengths of PE and PVC into an effective atomic number. The result is represented in the pseudo-colour image.

Since the equivalent lengths behave linearly, the estimated Z_{eff} is independent from thickness.

In the case of stacked materials the measured equivalent lengths are equal to the sum of the contributions from the different materials. Whenever one of the stacked materials can be measured separately, it is possible to deduce the equivalent lengths of the second material, and subsequently the Zeff. Only the small bias and noises are quadratically added. Therefore the quantum noise should be reduced as much as possible by increasing the photon statistic.

Another example of application of the decomposition method is the separation of the soft tissues and bone as shown in Figure 2. The spectral images were decomposed in PE and PVC. Soft tissues and bone have different attenuations from those of the base materials. We performed a linear combination of PE and PVC images to obtain a representation of soft tissues and bone. The contributions of both types of tissues are perfectly separated and the bone image provides a quantitative measurement of bone mineral density.

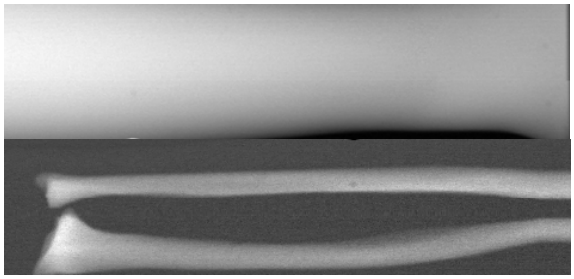

Figure 2: Soft tissue (top) and bone (bottom) image resulting from a linear combination of PE and PVC images.

Perspectives

We have shown that the proposed method can be used to identify and quantify plastic materials with close atomic number. It can easily be applied to all materials whose atomic number is between those of the two materials of the calibration base. When high Z materials are present, for instance with Iodine or Gadolinium in contrast enhanced k-edge imaging, a third calibration material is needed to take into account for the k-edge in the linear attenuation coefficients.

Related Publications:
[1] http://www.multixdetection.com/.
[2] A. Brambilla, P. Ouvrier-Buffet, G. Gonon, J. Rinkel, V. Moulin, C. Boudou, L. Verger, "Fast CdTe and CdZnTe Semiconductor Detector Arrays for Spectroscopic X-Ray Imaging", Nuclear Science, IEEE Transactions on , vol.60, no.1, pp.408,415, Feb. 2013.

High accuracy (100 electrons), low power, integrated circuit for X-ray medical imaging in spectrometric and integration modes

Research topic: X-rays, Medical imaging, Spectrometry, Integration

Authors: A. Habib, M. Arques, J.-L. Moro, M. Accensi, S. Stanchina, B. Dupont, G. Sicard, M. Tchagaspanian, L. Verger

Abstract: Multi-energy X-ray medical imaging (also called color imaging) allows distinguishing different components in a patient, such as bones, soft tissues, or injected products such as iodide or gadolinium. This has been up to now developed in X-ray CT scanners which use linear detectors. This project aims providing the same capabilities to a 2D flat panel detector used in conventional radiography. A small integrated circuit has been designed and tested. It includes a new pixel electronic concept mixing spectrometry and integration modes and offering a high accuracy quantification step (100+/-10 electrons) and less than 2µW/pixel analog power consumption.

Radiography X-ray medical imaging requires 2D large surface detectors (from 20 cm to 40 cm width) equipped with rather large pixels (from 50 µm to 200 µm width). Submicronic high integration integrated circuits allow designing complex circuitry in such pixels. The goal of this project is to implement a multi-energy discriminator in each pixel, thus allowing X-ray color imaging. The energy of each detected X-ray is measured and, depending on this measurement, one of a series of counters implemented in the pixel is incremented.

The detection process includes a first step where each X-ray is absorbed and converted in secondary particles (either visible photons if the absorber is a scintillator or electrons if the absorber is a photoconductor), and a second step, in an integrated circuit, where these secondary particles are measured to give the X-ray energy. The ASIC was designed with 100 electron quantification accuracy to match both scintillator or photoconductors approaches. In addition, as the global detector will include several million pixels, the power consumption of each pixel has to be kept as low as a few microwatts to fulfill the specification.

We have developed for several years [1] a concept of counter charge measurement (also called charge balancing). In this concept, the electrons created by the detection of an X-ray cause the decrease of the voltage of a capacitor. When this voltage crosses the threshold of a comparator, a positive calibrated counter charge is injected on the capacitor. This counter charge corresponds to the quantification step, and the number of counter charges required to compensate for the X-ray gives the digitized value of its energy.

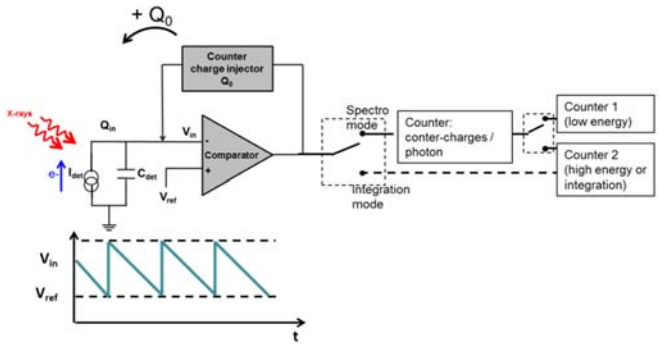

Figure 1: Integrated circuit pixel schematics.

The schematic diagram of the present circuit [2], called "Sphinx", is given in Figure 1. It has been designed with two main goals:

- Improvement of the previous ASIC in order to achieve lower and more homogenous values of the counter charges, thanks to a new readout technique,
- In case the X-ray flux is too high, the pulses corresponding to the different detected X-rays pile-up, and the spectrometric measurement is no more feasible. The integrated circuit then includes a mode where all counter charges are summed up independently on the X rays which have generated them. This is the so called "integration mode".

The ASIC was processed in a 0.13µm CMOS process. It includes a 20 × 20 pixel array, with design variations corresponding to 5 × 5 pixel sub-arrays.

The homogeneity of the quantification step is shown in Figure 2, with the old (left) and new (right) readout techniques. The new technique brings 100 electrons ± 10 electron accuracy in the quantification step, as expected, except on one of the sub-arrays. Power consumption of the analog part ranges from 1 to 2 µW/pixel, depending on the X-ray flux, as expected. Readout noise is higher than expected (80 electron noise instead of 20 expected electrons for 20 fF input capacitor), but cause has been identified and will be corrected in a next design.

Characterization of the integration mode is in progress.

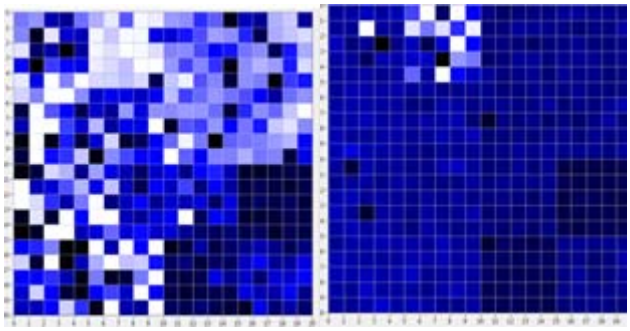

Figure 2: Homogeneity of the 100 electron quantification steps of SPHINX test ASIC, with the old (left) and new (right) readout techniques. The new technique brings 100 ± 10 electron quantification step.

Related Publications:
[1] A. Peizerat, M. Arques, P. Villard, J.-L. Martin, G. Bouvier, “Pixel-level ADC by small charge quantum counting”, in 13th IEEE International Conference on Electronics, Circuits and Systems, 2006. ICECS ’06, 2006, p. 423-426.
[2] A. Habib, M. Arques, B. Dupont, P. Rohr, G. Sicard, M. Tchagaspanian, L. Verger, "Sphinx1: Spectrometric photon counting and integration pixel for X-ray imaging with a 100 electron LSB", IEEE transactions on nuclear science, vol. 62, no. 3, june 2015.

Development and evaluation of a portable CZT coded aperture gamma-camera

Research topic: CZT detectors, Coded aperture, Gamma imaging

Authors: G. Montémont, L. Maingault, O. Monnet, S. Stanchina, L. Verger

Abstract: We present the design and the evaluation of a CdZnTe (CZT) based gamma camera using a coded aperture mask. This camera, based on a 8 cm^3 detection module, is small enough to be portable and battery-powered (4 kg weight and 4 W power dissipation). As the detector has spectral capabilities, the gamma camera allows isotope identification and colored imaging, by affecting one color channel to each identified isotope. As all data processing is done at real time, the user can directly observe the outcome of an acquisition and can immediately react to what he sees.

Context and Challenges

Gamma ray imaging is a well-established technique, used for a wide variety of applications. Gamma-cameras have been used for functional medical imaging since the 60's and are now widespread. Large scientific instruments like astrophysics gamma-ray observation satellites have been developed since the 80's (Compton Gamma Ray Observatory, CGRO). In the domain of nuclear industry and decommissioning, gamma imaging is not widely used for a variety of reasons: systems need to be easily moved, the measurement environment is often complex and variable from case to case. Imaging systems often lack of versatility to be easily used and their operation is often too complicated.

Main Results

Our gamma-camera is based on a 8 cm^3 CZT detector with 0.3 mm spatial resolution and 1.5% overall energy resolution at 662 keV. We have used deterministic coded aperture masks (hexagonal uniformly redundant array pattern). Mask deconvolution is performed using an iterative algorithm based on Maximum Likelihood Expectation-Maximization (MLEM) including a model of the detector, of the mask, of radioisotope signature and of background radiation.

Figure 1: Near real-life experimentation at JRC Ispra showing 3 radioactive sources hidden inside a car for customs usage scenario.

The algorithm operates at real time, in parallel of data collection. The object estimation progressively integrates newly collected data and the user is able to see the gamma image as soon as the number of collected photons is sufficient to distinguish something. A different color (red, green or blue) is attributed to each identified isotope.

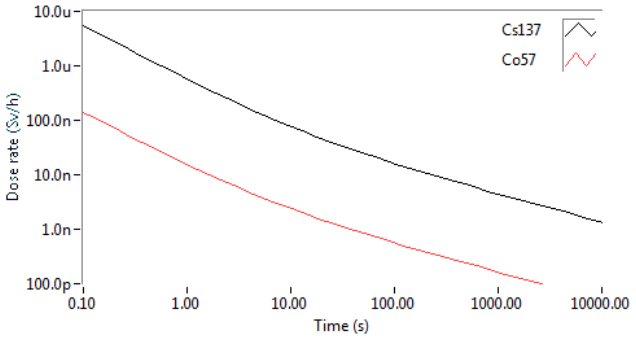

Figure 2: Evaluated sensitivity of the system for two common radioisotopes (Co-57 and Cs-137). This curve shows the minimal dose rate detectable in a given acquisition time for a natural background around 70 nSv/h.

Our system is sensitive enough to measure radiation level below background level. Within 30 seconds, it can localize a 0.1 MBq source of ^{57}Co at 1 m or a 1 MBq source of ^{137}Cs at 1 m, in the natural background of our laboratory (around 60 nSv/h). Angular resolution on the images is 2.5 degrees for a field of view of 40 degrees.

The energy resolution of the device offers two added values: first, it makes it possible to identify the radionuclide present in the image. Second, it improves detectability of a weak source hidden in a higher background because it can be spectrally isolated and not only spatially isolated. The combination of these two complementary information sources improves diagnosis quality.

Perspectives

As the developed system achieves a good trade-off between sensitivity and portability, we are currently improving its operational qualities by working on mechanics and software.

The aim is to have a compact easy to handle device with a seamless interface easy to use for a non-expert user and that could be operated from lightweight devices like a phone or a tablet.

Related Publications:

[1] G. Montémont, O. Monnet, L. Maingault, S. Stanchina, L. Verger, F. Carrel, V. Schoeppf, G. Ferrand and A.-S. Lallemand, “Development and evaluation of a portable CZT coded aperture gamma-camera”, ANIMMA 2015 conference record, Lisboa, Portugal.

[2] G. Montémont, S. Lux, O. Monnet, S. Stanchina, L. Verger, “Studying Spatial Resolution of CZT Detectors Using Sub-Pixel Positioning for SPECT”, IEEE TNS61, oct. 2014.

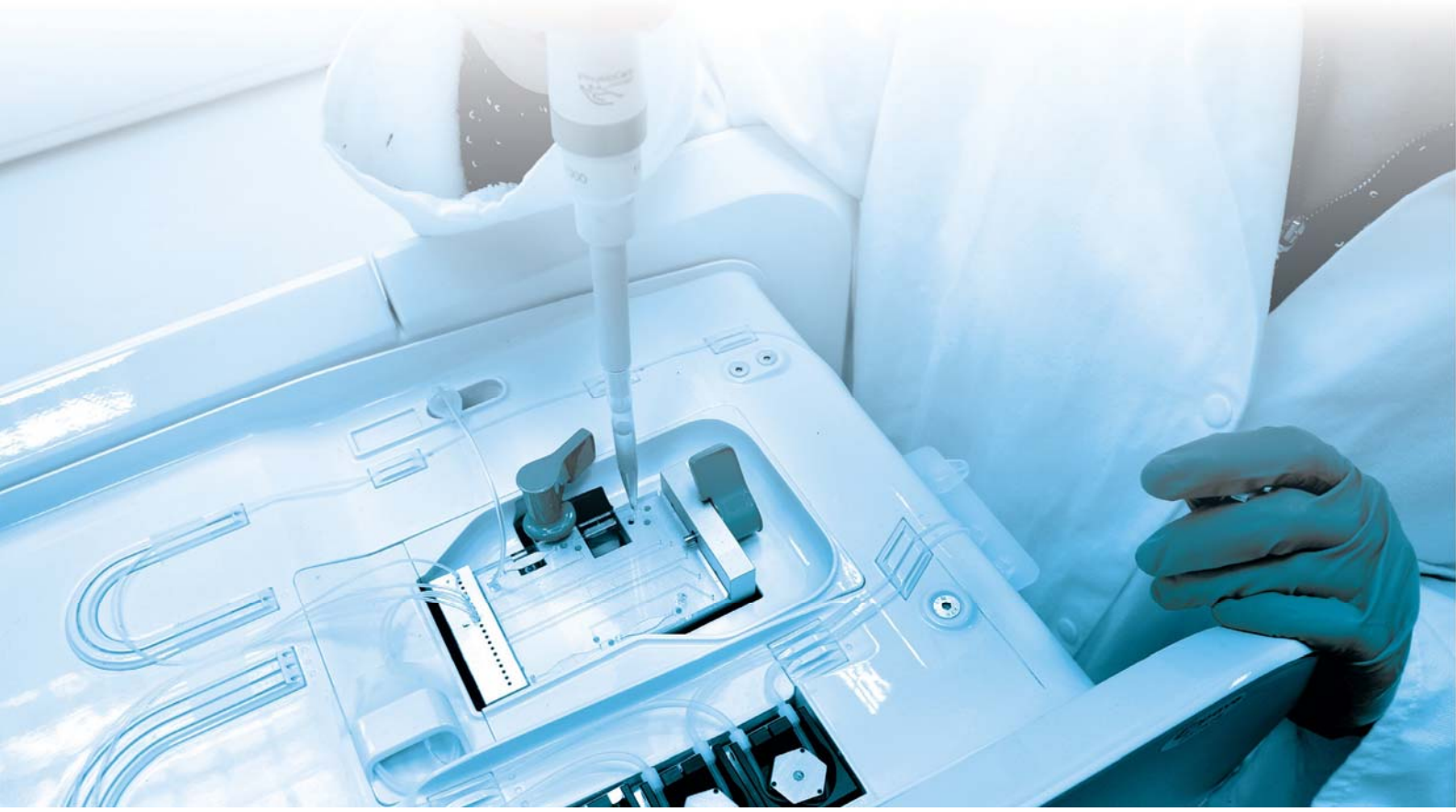

2

OPTICAL IMAGING

- Fluorescent imaging
- Raman spectroscopy
- Lensfree video microscopy
- Time-resolved tomography

Label-free investigation of type I collagen ageing in 3D matrix using confocal reflectance microscopy and diffuse reflectance spectroscopy

Research topic: Diffuse reflectance spectroscopy, Skin characterization, Skin ageing

Authors: B. Roig, A. Koenig, F. Perraut, J.-M. Dinten

Abstract: Our objective is to investigate the use of spatially resolved diffuse reflectance spectroscopy for skin ageing assessment by focusing on type I collagen as skin chromophore and scatterer. Measurements were carried out *in vitro* on 3D collagen matrices and *in vivo* on several volunteers' skin. According to the *in vitro* results, diffuse reflectance signal of type I collagen appears as a relevant marker for skin ageing assessment. The interpretation of the *in vivo* scattering spectra shows despite a great variability between subjects the same trend; that is a decline of scattering with skin age, not necessarily chronological age but at least mechanical.

Context and Challenges

The ageing process constitutes a field of major interest in our society since it represents a progressive, irreversible, and multidimensional mechanism affecting all people. First we investigated the influence of skin ageing *in vitro* in collagen 3D matrix model, using a combination of label-free biophotonic tools allowing to access complementary data. For that, confocal reflectance microscopy (CRM) was applied to image the different-age collagen 3D constructs, providing information on the microscopic organization of networks.
Complementarily, the 3D matrices were analyzed by diffuse reflectance spectroscopy (DRS) to determine their specific optical properties. And last, for *in vivo* experiments a cutometer allowed mechanical measurements of the skin.

Main Results

We studied the potential application and relevance of the DRS technology for skin ageing assessment first by focusing on type I collagen as skin chromophore and scatterer. Native type I collagen was extracted from rat tail tendons of different-age animals (newborn, young adults of 2 months and 2 years old adults). We generated reconstituted collagen hydrogels and the DRS measurements were done over each. The curves shapes of Figure 1 presents the scattering spectrum obtained with DRS on the different collagen matrices. We observe significant differences between extracted collagen from young and old rats. The newborn curve is itself quite different. This is assessed by the CRM measurements and structures of collagen fibrils.

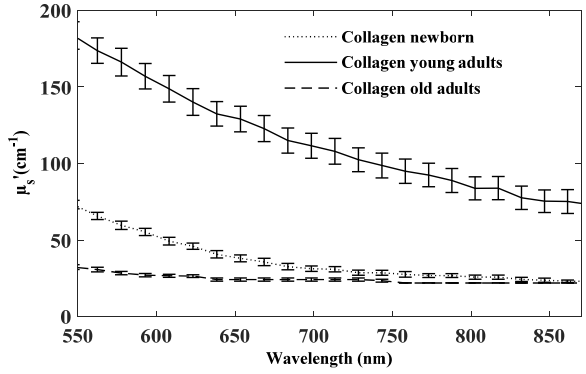

Figure 1: DRS scattering spectrum obtained on matrices of different ages collagens.

This result confirms the suitability of scattering properties extracted by DRS of type I collagen as an *in vivo* marker of skin ageing. We pursued the study with *in vivo* experiments on a panel of volunteers representative of different ages. The discrimination between the youngest and oldest volunteers from scattering spectra extracted by DRS is not as straightforward as for *in vitro* scattering spectra. In fact there is a great difference between the age of the panelists and skin ageing. For this reason, we focus the study on the inside of forearm to limit effect of photo-ageing due to exposure to UV rays. Furthermore, we use a mechanical measurement to estimate skin age (mechanical) rather than panelist age (chronological). Panelist skins were analyzed with a cutometer. The R7 parameter measures the ability of the skin to return to its initial state after morphological elongation. The scattering coefficient extracted by DRS is then studied against this R7 parameter, see Figure 2. We do not observe significant differences between young and intermediate skin scattering levels. In contrast, the sensitivity level of aged skin is much lower than the two other groups.

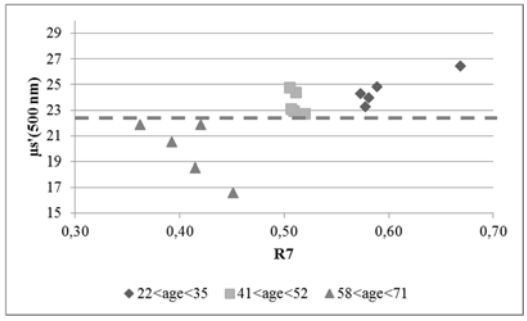

Figure 2: Reduced scattering coefficient @ λ = 500 nm obtained by DRS depending on the R7 cutometer parameter.

Perspectives

Using DRS technology to study the skin, we found a wide variability of scattering properties of the skin of an individual to another. This variability depends on the analyzed area (face or forearm, epidermis or dermis + epidermis), but also structural and physiological variation inter-individual. Within the potential sources to explain these variations we identified skin ageing and especially degradation of the dermis collagen network with the age.
This work forms integral part of Blandine Roig's PhD work.

Related Publications:
[1] M. Guilbert, B. Roig and al., "Highlighting the impact of ageing on type I collagen: label-free investigation using confocal reflectance microscopy and diffuse reflectance spectroscopy in 3D matrix model", Oncotarget. 2016 Feb 14. doi: 10.18632/oncotarget.7385.
[2] B. Roig, "Caractérisation de tissus cutanés par spectroscopie bimodale: Réflectance Diffuse et Raman", Thèse de l'université de Reims champagne Ardenne soutenue le 19/11/2015.
[3] A. Koenig, S. Grande, K. Dahel, A. Planat-Chrétien, V. Poher, C. Goujon, J-M. Dinten, "Diffuse reflectance spectroscopy: a clinical study of tuberculin skin tests reading", BiOS, 2 - 7 February 2013, San Francisco, California USA.

A study on identification of bacteria in environmental samples using single-cell Raman spectroscopy: feasibility and reference libraries

Research topic: Confocal raman, Micro spectroscopy, Single cell identification, Chemometrics

Authors: J.-C. Baritaux, A.-C. Simon, E. Schultz, C. Emain, P. Laurent, J.-M. Dinten

Abstract: We report on our recent efforts towards identifying bacteria in environmental samples by means of Raman spectroscopy. We demonstrated the feasibility of Raman typing from measurements performed in non-ideal conditions, and investigated the identification robustness to deviations between conditions included in the statistical model and conditions of the sample.

Context and Challenges

Raman spectroscopy is gaining popularity in bacteria monitoring applications, in particular for biological threat detection activities. However, samples investigated in this context are complex, both in terms of phenotype content and environmental matrix. The promise of culture-free identification of bacteria in environmental samples by Raman spectroscopy is thus largely conditioned upon our ability to build robust statistical models with sufficient coverage. The purpose of this study is twofold. First, verify the feasibility and robustness of bacteria identification performed in non-ideal conditions and second, investigate the content required in the training set of the chemometric model used for identification.

Main Results

A comprehensive database of single-cell Raman spectra was collected on a panel of five bacteria species (*B. cereus*, *B. subtilis*, *S. epidermidis*, *E. coli*, *S. marcescens*). In these experiments the cells were first cultured in standard conditions (supplier specified), then submitted to various growth conditions (medium and temperature) and finally embedded in two environmental matrices relevant to field applications: a solution of atmospheric air dissolved in water (AIR), and condensed water from a cooling tower filtration system (TARH). The collection of spectra was acquired over the course of several months (3 to 10) using a custom Raman instrument recently developed in our lab [1]. A statistical model was trained on this dataset after spectra had been pre-processed, and classification (SVM) was performed at the species level. Datasets acquired in heterogeneous conditions. It is essential to ensure consistency of the data entering the statistical model, both globally, and condition-wise. In our case this was implemented by applying an outlier detection procedure to the data [2]. With this approach, stable classification results were obtained on data assembled over a 10-months period (Figure 2). Considering ideal lab culture conditions, a mean correct classification rate of 96.8% is obtained at the species level, which is in accordance with performance generally reported in the literature. Figure 1 shows the identification results obtained when the conditions (both in terms of phenotype and matrix) are altered. The influence of several training sets is also examined. We started with a condition-specific model trained on a dataset matching at best the sample conditions (STD).This approach lead to very satisfying identification results on a panel of five species measured directly in two environmental matrices relevant for field applications: atmospheric air dissolved in water, and condensed water from a cooling tower.

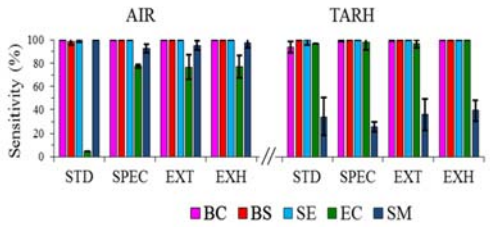

Figure 1: Classification of BC, BS, SE, EC and SM measured in AIR and TARH environmental matrices. Sensitivity and standard deviation are represented. Standard (STD), Specific (SPEC), Extended (EXT), and Exhaustive (EXH) training sets are evaluated. SPEC is composed exclusively of spectra from the same conditions as the test set.

Yet, difficulties appeared for the bacteria with the closest spectral signatures (EC and SM in our bacteria panel). This suggests a tradeoff between sample preparation and direct in-situ measurements, especially when bacteria are embedded in the TARH matrice since it contains a high amount of impurities. We then varied the diversity content of the training set, with the goal of building a model with broad coverage. Two limit cases were considered: the least amount of diversity (STD), and all the diversity available (EXH). Interestingly, the model with least amount of diversity (trained solely on standard spectra) was sufficient to classify the most spectrally-distinct bacteria, independently of their conditions. The exhaustive model, on the other hand, resulted in very satisfying performance on the entire dataset. This last approach is promising for environmental samples since the investigated phenotype, or environmental matrix may be missing from the training set and need to be approximated.

Perspectives

The results of this study will help refining the content of a bio-pathogens reference library currently under construction. By carefully selecting a library that accounts for the spectral distances between the pathogens of interest, as well as spectral variabilities resulting from non-ideal measurements, we anticipate that our Raman instrument will efficiently integrate the chain of analytical tools deployed in the field in response to biological threat.

Related Publications:
[1] S.A. Strola, J.-C. Baritaux, E. Schultz, et al (2014), “Single bacteria identification by Raman spectroscopy”, J Biomed Opt. doi: 10.1117/1.JBO.19.11.111610
[2] J.-C. Baritaux, A.-C. Simon, E. Schultz, P. Laurent, C. Emain, J.-M. Dinten, “A study on identification of bacteria in environmental samples using single-cell Raman spectroscopy: feasibility and reference libraries”, Environ Sci Pollut Res Int. 2015. DOI: 10.1007/s11356-015-5953-x, ESPR-D-15-03270.1.

Dynamics of cell and tissue growth acquired by means of extended field of view lensfree microscopy

Research topic: Medical optics and biotechnology, Cell analysis, Tissue characterization

Authors: F. Momey, J.-G. Coutard, T. Bordy, F. Navarro, M. Menneteau, J.-M. Dinten, C. Allier

Abstract: A new methodology based on lensfree imaging allows to perform wound healing assay with unprecedented statistics. Our video lensfree microscopy setup is a simple device featuring only a CMOS sensor and a semi coherent illumination system. Yet it is a powerful mean for the real-time monitoring of cultivated cells. It can perform the follow-up in a large field of view of 25 mm^2 and final point imaging over extended field of view of 10 cm^2. We have assessed this methodology to perform label-free measurements of the velocities of the fronts of proliferation of the cell layer as a function of time by means of particle image velocimetry (PIV) processing.

Context and Challenges

In the context of tissue growth experiments such as wound healing assays, lensfree imaging offers the possibility to follow and quantify the proliferation of a cell layer at the tissue's scale. We first address this point by measuring the velocities of the fronts of proliferation of the cell layer by means of particle image velocimetry (PIV) processing on lensfree sequences. Still measurement biases could appear due to positioning the sensor at an irrelevant area. Hence it would be interesting to enlarge it again and be able to visualize the entire surface of proliferation of the cell culture, e.g. a Petri dish or a well plate. Consequently, we have developed a setup for addressing this challenging task. We have mounted the source/sensor couple on motorized XY stages, in order to acquire different positions of the field of interest. As a result we are able to scan and recombine in a single image the entire surface of interest, i.e. the entire available area for the proliferation of the seeded cell population (about 10-20 cm^2), in about 10 minutes (scan + image recombination), with the same resolution as our first lensfree device.

Main Results

In this paper [1], we have demonstrated a new methodology using real-time label-free lensfree imaging and PIV processing (Figure 1) for quantifying the local velocities of the proliferation fronts of a cell layer over a large field of view (25 mm^2). Such measurements are performed on much larger areas in comparison with classical microscopy (x10) and can be followed over large periods of time. We have also reported a proof of concept of an extended field (10-20 cm^2) lensfree scanner for imaging in cell biology (Figure 2). With such a device, we address the problem of a wrong positioning of the imaging system to an irrelevant field of view of the cell culture, by rapidly acquiring a meta-image of the entire area of interest with the same resolution as our known lensfree video microscopy device. We have tested our methodology on wound healing assays of cultures of keratinocytes HaCaT in Petri dishes. We coupled the scanning setup with real-time lensfree video microscopy (25 mm^2) to monitor the experiments in time and get a measure of velocimetry (PIV) of the fronts of proliferation. These preliminary works have highlighted the great interest of combining in a single device, extended field of view fast acquisitions with real-time monitoring inside the incubator.

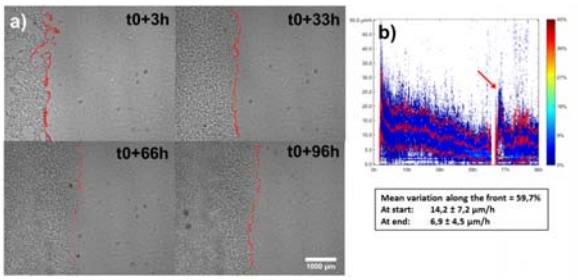

Figure 1: (a) Real-time lensfree sequences of of HaCaT cultures and its respective scatter graphs of distributions of proliferation velocities over time (b) as measured with PIV methods. The red curves corresponds to the mean velocity (solid) ± its standard deviation (dash). Blanks correspond to loss of acquisition. The red arrows on the graphs identify dates corresponding to the addition of culture medium.

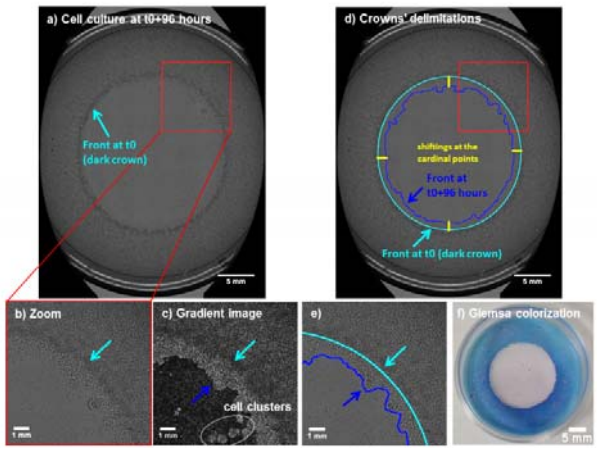

Figure 2: Label-free measurement of the area of proliferation on the lensfree scan of the entire Petri dish of the HaCaT culture. (a) Meta-image at t0+96 hours. (b) Zoom on a region of interest. (c) Gradient image. The clusters corresponds to the growth of cells ripped at the removing of depletion plot. (d) Crowns' delimitations at t0 and t0+96 hours for areas' measurements. (f) Colorized Petri dish for classical non label-free measurements of proliferation.

Perspectives

Our long-term objective is to couple extended field and real-time imaging inside the incubator on a single scanning device.

Related Publications:
[1] F. Momey, J.-G. Coutard, T. Bordy, F. Navarro, M. Menneteau, J.-M. Dinten, C. Allier, (2015, February), "Dynamics of cell and tissue growth acquired by means of 25 mm² to 10 cm² lensfree", SPIE BiOS conference, Imaging, Manipulation and Analysis of Biomolecules, Cells, and Tissues XIII.

Lensfree diffractive tomography for the imaging of 3D cell cultures

Research topic: Lensfree diffractive tomography for 3D microscopy

Authors: F. Momey, A. Berdeu, T. Bordy, J.-M. Dinten, F. Kermarrec Marcel, N. Picollet-D'hahan, X. Gidrol, C. Allier

Abstract: A new imaging platform based on lensfree microscopy is presented: a lensfree diffractive tomography setup performing multi-angle acquisitions of 3D organoid culture. Dedicated 3D holographic reconstruction algorithm based on the Fourier diffraction theorem are developed. With this new imaging platform, we have been able to reconstruct a 3D volumes bigger than 20 mm^3. Comparisons with 2D images show that it is possible to resolve single cells isolated from the main cellular structure with our lensfree diffractive tomography setup.

Context and Challenges

New microscopes are needed to help realize the full potential of 3D organoid culture studies by gathering large quantitative and systematic data over extended period of time while preserving the integrity of the living sample. On another hand, lensfree video microscopy is addressing these needs in the context of 2D cell culture, providing label-free and non-phototoxic acquisition of large datasets. As scientists routinely adopt 3D culture techniques, the new challenging task is to extend lensfree microscopy techniques to 3D structures.

Main Results

Unlike 2D lensfree imaging, where only one image is required for retrieving the 2D object, the reconstruction of a 3D object from lensfree acquisitions requires to multiply the viewing angles. For this purpose, we have developed experimental benches composed of a semi-coherent illumination source and a CMOS sensor [1]. The object is placed on top of the sensor at a distance of 1 to 3 mm, the illumination being tilted relative to the sensor (Figure 1-a). This configuration is the most adapted to 3D organoid culture in standard containers such as Petri dish or well plates. The incident wave is diffracted by the sample and the sensor records the resulting hologram.The object is retrieved based on multiple acquisitions at different angles, using the Fourier diffraction theorem [2]. The Fourier transform of each diffracted wave is mapped on a spherical cap in the 3D Fourier domain of the object to reconstruct. This cap depends on the lighting position and the illumination wavelength. An inverse Fourier transform is the final step to get an estimation of the 3D diffracting object.

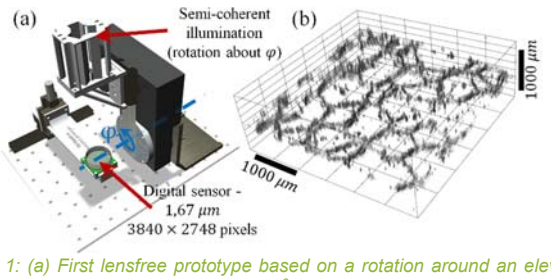

Figure 1: (a) First lensfree prototype based on a rotation around an elevation angle. (b) 3D view of a 4 x 4 x 1.34 mm^3 volume of a culture of prostatic cells RWPE1 assembling in 3D intricate cellular network at the mesoscopic scale.

A first prototype allowed us to acquire multi-angles data on a culture of prostatic cells RWPE1 in Matrigel® and to reconstruct a large volume of 4 x 4 1.34 mm^3 showing that cells interestingly tend to form a structured network (Figure 1-b).

A comparative study with 2D reconstructions from 2D lensfree data acquired at the normal illumination was conducted showing the ability to recover cell-sized object despite twin-image and reconstructions artefacts. Thus on the xy plane the resolution is sufficient enough to resolve 15µ m objects. On the z-axis, the resolution deteriorates up to ~200µm depending on the position in the field of view.

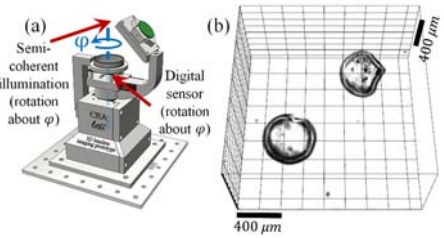

Figure 2: (a) Second lensfree prototype based on a rotation around an azimuthal angle. (b) 3D view of a 1710 x 1710 855 µm^3 volume of beads embedded in matrigel® capsules.

A new prototype was developed to increase the resolution on the z-axis, while increasing the angular coverage (Figure 2-a). Some data were acquired on beads embedded in Matrigel® capsules. The first reconstructions seem promising, while the beads are easily detected and positioned inside the capsules (Figure 2-b). These first results tend to demonstrate that it is possible to acquire knowledge on the positions and shapes of elements present in 3D cell culture, e.g. spheroids, branching and single cells, on a large and thus relevant volume (several mm^3. Acquiring such information is of prior importance for the biologists in the realms of e.g. embryogenesis, angiogenesis and tumorigenesis. In particular the ability to detect isolated single cell distant from the main cell structure, since these cells may present a metastatic phenotype of interest.

Perspectives

On the one hand, the incoming research will focus on improving the reconstruction algorithm with inverse problem methods and regularisations. A better phase retrieval and adapted regularisation will erase the twin-image and reduce artefacts due to the lack of angles. On the other hand, the prototypes will be adapted to resist incubator conditions to get 3D video-microscopy on living biological samples.

Related Publications:
[1] F. Momey and al, "Lensfree diffractive tomography for the imaging of 3D cell cultures", Gretsi, Lyon Sept. 08-11th 2015.
[2] E. Wolf, "Three-Dimensional structure determination of semi-transparent objects from holographic data", Optics communications, 1(14), 153–156 (1969).

Towards non-invasive assessment of flap viability with time-resolved diffuse optical tomography: a pre-clinical test on rats

Research topic: Time- resolved Optical Diffuse Tomography and Spectroscopy, Flaps viability

Authors: L. Di Sieno, G. Bettega, M. Berger, C. Hamou, M. Aribert, A. Puszka, H. Grateau, L. Hervé, J.-M. Dinten, A. Planat-Chrétien

Abstract: We present a new setup for time-resolved diffuse optical tomography based on multiple source-detector acquisitions analysed by means of "Mellin-Laplace transform". The proposed setup has been used to perform pre-clinical measurements on rats in order to show its suitability for non-invasive assessment of flap viability.

Context and Challenges

In reconstructive surgery anatomical defects are often restored using autologous tissues ("flaps"). It's fundamental for the flap survival that arteries and veins are well reconnected and no vessels obstruction occurs. Indeed, the major complication of this type of surgery is thrombosis which can cause the fail of the flap and the consequent necrosis of tissues. In order to save the flap it is fundamental to rapidly restore the vessel permeability. For an early diagnosis, various instrumental techniques have been developed but none are used routinely. Some of them are invasive and have limited depth sensitivity. This is a critical point since flap can be 1.5 to 3 cm thick and they can also be buried under 1.5-2 cm of fat, muscle and skin. For this reason, the capability of investigate deep layers is a fundamental.

Main Results

We developed a "Time-Resolved Near-Infrared Spectroscopy" (TR-NIRS) system to non-invasively evaluate the deep perfusion in tissues in reflectance geometry. Indeed, photons that arrive later are those that travelled most in depth, thus retrieving information about oxygenation of deep layers. In addition, it has been demonstrated that the use of a small distance between injection and collection fibers using a reflectance geometry allows to increase both spatial resolution and the overall number of detected photons without any degradation of depth sensitivity [1], provided that time-gated acquisition are employed to reject the overwhelming number of early photons coming from superficial layers of the tissue under investigation. In [2] we presented a setup for Diffuse Optical Tomography based on small source-detector distance and high-dynamic range measurements [3] acquired by means of a fast-gated Single-Photon Avalanche Diode (SPAD) and analysed using the Mellin-Laplace transform (MLT) and there we demonstrated an increased spatial resolution. In this work we present a system based on fast wavelengths multiplexing for improving the reconstruction of changes in oxygenation in depth (see fig1). A pre-clinical study on rats abdominal fascio-cutaneous flaps has been performed so as to prove the suitability of this technique to the non-invasive monitoring of flap. Schematic of the experimental setup (left), position of source in the operated mouse (middle) and reconstructed volume with axes and representation of xy and yz planes (right) are figured in Figure 1. The DOT image reconstruction method is described in [4,5]. It is applied on the reconstructed high-dynamic range curves provided by fast-gated acquisitions [3].

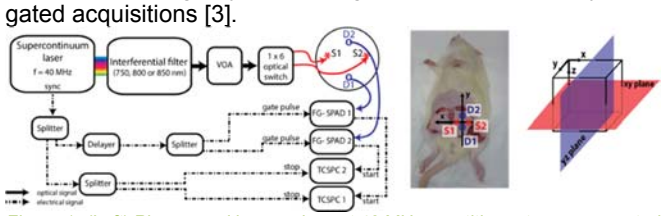

Figure 1: (Left) Picosecond laser pulses at 40 MHz repetition rate are generated by a supercontinuum fiber laser (Fianium LDT, London, UK). The wavelength is selected by means of three interferential filters centered at 750 nm, 800 nm and 850 nm and mounted on a motorized wheel (software controlled). Light exiting from the interferential filter is then attenuated by means of a motorized Variable Optical Attenuator (VOA) and sent into a 1x6 optical fiber switch (core size: 62.5 µm). (Middle): Position of the probe in the operated mouse, (Right): reconstructed volume.

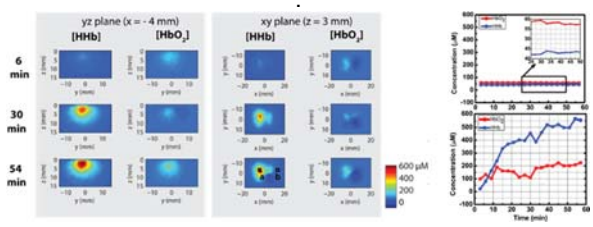

Figure 2: venous occlusion: Maps of HHb concentration in the yz plane (x = -4 mm) and xy plane (for z = 3 mm) and time evolution of HHb and HbO2 concentrations in two different regions (named a and b).

We simulated both venous and arterial occlusion (only venous occlusion shown here) and obtained 3D maps of concentration of HHB and HbO2 in the tissue (Figure 2 - left) with expected time evolution of these concentrations (Figure 2: right). Thus we validated on very preclinical *in vivo* measurements on 4 rats the capability of our set-up to monitor non-invasively the flap viability based on fast gated optical tomography.

Perspectives

Thanks to the positive results obtained on rats, we will focus now on an animal model closer to the human for flap thickness which is much higher (1-3 cm) than that of rats (pig model). In this case the improvement in depth sensitivity due to fast-gated technique will be a fundamental feature. Future works will also consider the optimization of the probe and the increase in source detectors couples in order to improve 3D reconstruction of HHb and HbO2.

Related Publications:
[1] A. Puszka, L. Di Sieno, A. Dalla Mora, A. Pifferi, D. Contini, G. Boso, A. Tosi, L.Hervé, A. Planat-Chrétien, A. Koenig, J.-M. Dinten, "Time-Resolved Diffuse Reflectance Using Small Source-Detector Separation and Fast Single-Photon Gating" Phys. Rev. Lett. 100, 138101 (2008).
[2] A. Puszka and al., "Time-resolved diffuse optical tomography using fast-gated single-photon avalanche diodes", Biomed. Opt. Express 4, 1351 (2013).
[3] A. Tosi and al., "Fast-gated single-photon counting technique widens dynamic range and speeds up acquisition time in time-resolved measurements", Opt. Express 19, 10735–46 (2011).
[4] L. Hervé and al., "Time-domain diffuse optical tomography processing by using the Mellin-Laplace transform", Appl. Opt. 51, 5978–88 (2012).
[5] A. Puszka and al., "Time-domain reflectance diffuse optical tomography with Mellin-Laplace transform for experimental detection and depth localization of a single absorbing inclusion", Biomed. Opt. Express 4, 569–83 (2013).

Time Resolved optical detection for white mater lesion detection: preclinical tests on macaque brains and MRI co-registration

Research topic: Time-resolved optical diffuse tomography, Brain applications

Authors: A. Planat-Chrétien, M. Berger, L. Hervé, J.-M. Dinten

Abstract: We conducted a preclinical assessment on young macaques aimed at detecting white matter lesions. We present the protocol we implemented to achieve the lesions detection using a bedside non-invasive optical-based Time-Resolved instrumentation we have optimized for this purpose. We validated the reconstructed 3D absorption map with co-registration of MRI data.

Context and Challenges

Despite progresses made in neonatology, white matter lesions of the premature remain a major issue given the frequency of premature births and the poor cognitive prognosis associated in long term with such lesions for which there is today no preventive or curative treatment. In this context, we designed a bedside noninvasive optical-based instrument that aim at providing such information safely and continuously specially around the first week of life of the preterm babies. The system is based on a Time-Resolved instrumentation described in [1], coupled with a method based on Mellin-Laplace Transform [2] to reconstruct 3D optical characteristics deeply buried in diffusive tissues. For the purpose of the study presented here, we optimize the lab prototype in order to push it out of the lab and to address the operating room environment. A mobile secure instrument is built up to achieve pre-clinical tests in real surgery context. We present here the very first *in vivo* experiment to address the detection and identification of white matter lesion in young non-human primates (NHPs).

Main Results

To conduct these preclinical assessments, we developed the lesion model itself in NHPs. White matter lesion was performed in 4 Macaca cynomolgus of 17± 2 month-old by injecting through stereotactic guidance and after MRI 100 µl of L-α-phosphatidylcholine (LPC from Sigma at 2% diluted in sterile NaCl isotonic) at the speed of 10 µl/min in the sub-cortical white matter of the right parietal lobe (post-central gyrus, Broadman area 2 and 3). The LPC-induced lesions of the white matter is expected to be maximal, 8 days after injection. The study validated this lesion model in NHPs (see Figure 1a): a myelin loss – with necrosis sometimes - as well as a local inflammation was observed by LFB (Luxol Fast Blue) and H&E (Hematoxylin and Eosin stain) respectively. Nevertheless the quantification of these lesions leads to smaller volumes than expected: it was about 2 to 18 mm3, instead of 1 cm^3 targeted, which means it may be undetectable in some cases.

The system we optimized to performe TR- measurements is more detailed in [3]. To achieve the co-registration of MRI data and optical acquisitions, we build a common reference framework based on a stereotaxic frame. MRI and optical signals are acquired before (normal state) and after LPC injection (lesion).

The reconstruction processed in two steps:
first a 3D map of the normal state, followed by the 3D map of the lesion state. The lesion itself resulted as the difference between both. A good correlation between optical measurements and MRI data was observed. The scar on the scalp (due to cranial LPC injection), when present in the measurement field, was clearly co-registered for both modalities (Figure 1: example on NHP#2). Moreover the good co-localization of the MIR and optical data, we showed that the temporal approach was absolutely necessary to cope with coupling effects from one phase to another. Finally we detect 3 lesions and scars, one NHP was considered as a control since the lesion was too small (1 mm^3).

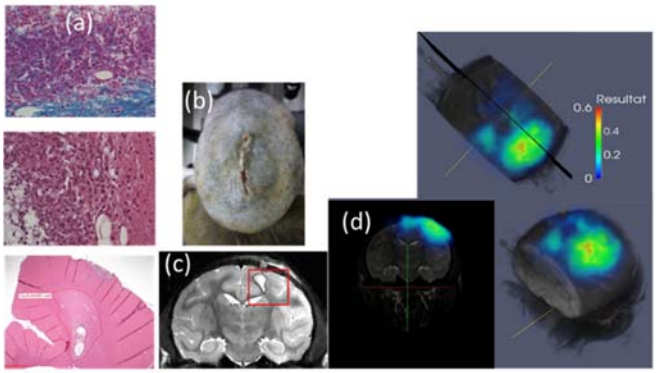

Figure 1: (a) Bottom: H&E; inflammation zone, necrosis with cavity. Middle and top LFB analysis: macrophages around the necrosis with a myelin loss (b) Presence of a scar in the measuring field of view (c) Lesion seen in MRI (d) Fusion of MRI and absorption 3D map on NHP#2).

Perspectives

We have developed a bedside non-invasive TR-instrument and validated its use for brain imaging purpose on 4 young NHPs. We provided co-registered MRI and optical data showing the ability of the system to localize properly pathological events. Optimization of lesion volume is underway and further experiments are scheduled to address the detection and precise localization of the white matter lesions with the scar out of the measurement field. Finally we focus on a new multispectral approach that get rid of the preliminary acquisition of signals on macaques having no lesion.

Related Publications:
[1] A. Puszka and al., "Time-domain reflectance diffuse optical tomography with Mellin-Laplace transform for experimental detection and depth localization of a single absorbing inclusion", Biomed. Opt. Express 4, 569–83 (2013).
[2] L. Hervé and al, "Time-domain diffuse optical tomography processing by using the Mellin-Laplace transform", Appl. Opt. 51, 5978–88 (2012).
[3] A. Planat-Chrétien, M. Berger, L. Hervé, L. Watroba, J. Demilly, J. Flament, L. Stimmer, P. Aubourg, J.-M. Dinten, "Time Resolved optical detection for white matter lesion detection: preclinical tests on macaque brains and MRI coregistration", Diffuse Optical Imaging V, SPIE Proceedings (Optical Society of America, 2015), paper 953806 (2015).

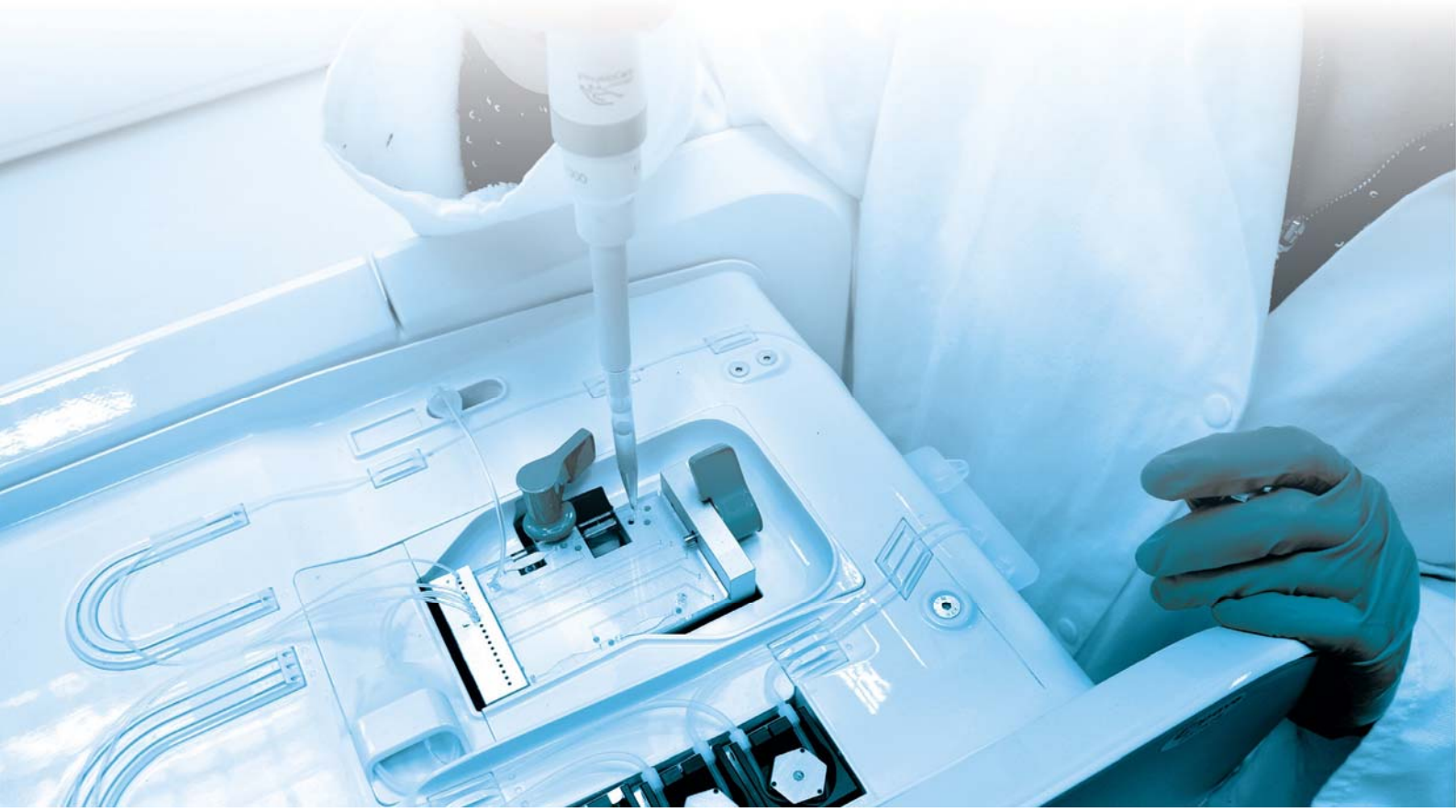

3

LAB ON CHIP

- Particule sampling
- Porous sensor
- Capillary-base microsystems
- Gas chromatography

ALEC PROJECT: Development of a new phase for lab-on-a-chip extraction of polycyclic aromatic hydrocarbons from water

Research topic: LOC, Water analysis, Porous SiOCH, Sensors

Authors: L. Foan, J. El Sabahy, F. Ricoul, A. Bellemin-Comte, B. Bourlon, S. Vignoud

Abstract: To date no portative equipment enables in situ determination of polycyclic aromatic hydrocarbons (PAHs) in environmental waters, with adequate selectivity and sensitivity. In this paper we report the development of a novel lab-on-a-chip for the PAHs extraction, destined to integrate field analysis portable system. Thanks to the use of a new phase, porous SiOCH, strong affinity for all PAHs is demonstrated, even in natural water. Very fast extraction time (20min) is also observed. Porous SiOCH extraction microchips therefore appear as a good alternative to PDMS-based extraction techniques such as SBSE and should be used for further development of field analysis devices.

Context and Challenges

Polycyclic aromatic hydrocarbons (PAHs) are considered to be persistent organic pollutants (POPs) due to their slow rates of degradation, toxicity and potential for both long-range transport and bioaccumulation in living organisms. These compounds have thus to be monitored in environmental waters or in water intended for human consumption. So far analysis are performed in laboratory which imply important costs and labor, and require sampling, transport and storage steps which can induce biases on the final results due to analyte loss or sample contamination [1]. Yet no portable solution assures selective measures of all PAHs at sub-µg/L levels. In this context, our team has developed a miniaturized pre concentration device intended to be used in a portable system for monitoring PAHs directly in environmental waters. It consists of a silicon/glass microfluidic device functionalized with an adequate chemical layer for PAH extraction and concentration (see Figure 1). A first study evaluated the performances of a lab-on-a-chip functionalized with polydimethylsiloxane (PDMS) in comparison with Stir-Bar Sorptive Extraction (SBSE), a reference method based on extraction by sorption of dissolved compounds from the aqueous phase by a magnetic bar covered with PDMS [2]. Encouraging results were obtained. However, the performance of the microchip had to be improved for the lightest PAHs (2-3 aromatic rings).

Main Results

The present work presents the results obtained with a new extraction phase: porous silicon organosilicates (SiOCH). These materials are deposited by a porogen approach [3] and were developed previously in the microelectronics field as low-dielectric constant materials used in interconnects, but they had never been used as an extraction phase prior to chromatographic analysis.

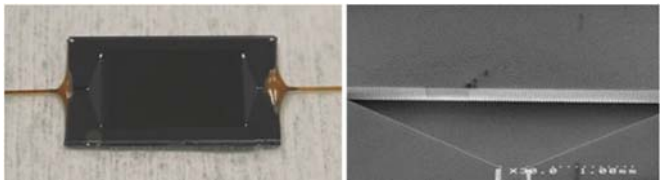

Figure 1: Left: Picture of the optimal chip with glued capillaries (outer dimensions: 2.1 x 1.2 cm); Right: SEM view of the microfluidic chamber entrance and the micropillars array (view from above before sealing).

After optimization of the microchip design and the operational parameters, equivalent recoveries with microchips functionalized with this phase to SBSE were obtained for all PAHs when extracting 10 mL of a 5 µg/L spiked solution, with an excellent extraction time of 1 min (Figure 2). Moreover, our device showed interesting performances with real environmental waters: due to the high surface area of the microchip, competition between the matrix and the analytes is reduced. The developed phase also presents the benefit of being applicable by full-wafer functionalization, a process which reduces manufacturing time and labor, and improves chip to chip reproducibility.

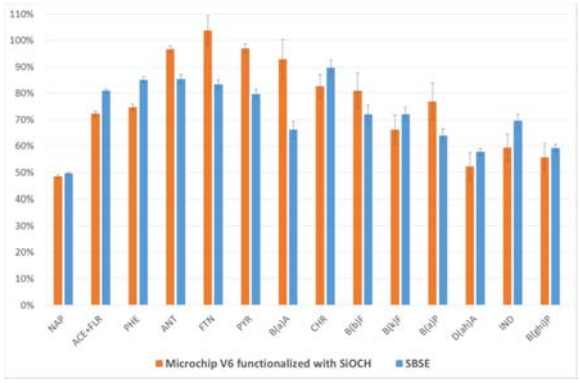

Figure 2: Comparison of the extraction recoveries obtained with the optimal lab-on-a-chip functionalized with porous SiOCH and SBSE. Tests were carried out with milli-Q water spiked with 5 µg L-1 of 16 PAHs. Error bars represent the standard deviation for n=3 measures.

Perspectives

Porous SiOCH coated lab-on-chips are promising devices which could be integrated in portable systems for direct analysis of PAHs in natural waters. The affinity of porous SiOCH for other organic compounds such as PCBs, PCDD/Fs, PBDEs, as well as pesticides and pharmaceutical compounds of intermediate polarity (log K_{OW} = [3-5]) should also be studied in aim to develop a new multi-residue extraction technique.

Related Publications:
[1] L. Wolska, M. Rawa-Adkonis, J. Namieśnik, "Determining PAHs and PCBs in aqueous samples: finding and evaluating sources of error", Analytical and Bioanalytical Chemistry 382 (2005) 1389-1397.
[2] L. Foan, F. Ricoul, S. Vignoud, "A novel microfluidic device for fast extraction of polycyclic aromatic hydrocarbons (PAHs) from environmental waters – Comparison with stir-bar sorptive extraction (SBSE)", International Journal of Environmental Analytical Chemistry (2015), DOI: 10.1080/03067319.2014.994617.
[3] A. Grill, V. Patel, "Ultralow-k dielectrics prepared by plasma-enhanced chemical vapor deposition", Appl. Phys. Lett. 79 (2001) 803-805.

Bioaerosol sampling

Research topic: Lab-on-chip, Air sampler

Author: J.-M. Roux

Abstract: Airborne particles are known to cause illness and to influence meteorological phenomena. A challenge is to collect micro and nanoparticules, microorganisms as well as toxic molecules with a device as simple and small as possible to be used easily and everywhere. Electrostatic precipitation is an efficient method to collect all kind of airborne particles. Furthermore this method can be miniaturized. A portable, silent, and autonomous air sampler based on this technology is therefore being developed with the final objective to collect very efficiently airborne pathogens such as supermicron bacteria but also submicron viruses.

Context and Challenges

Human exposure to airborne biological agents, especially to pathogenic organisms or allergenic particles is known to cause various illnesses, infections and allergies. Also, there is a great concern that biowarfare agents can be intentionally released with the purpose of causing public anxiety, sickness and fatalities. Safeguarding a certain area regarding bio-agents demands the detection of pathogenous vegetative bacteria, spores and viruses by sampling and analysing aerosols to trigger an alarm.

Main Results

Electrostatic sampling is one of the most efficient ways to collect particles by charging the aerosols and collecting them due to electrostatics forces. Samplers based on this principle were mainly developed as air cleaners. Recently it was shown to be a suitable method to collect micro-organisms and several devices were built to investigate their performance [1] to collect airborne microorganisms. Furthermore Quinton *et al.* [2] demonstrated that it is possible to produce an air flow and to capture particles by using physical phenomena induced by high voltage: air flow production by ionic wind and electrostatic capture.

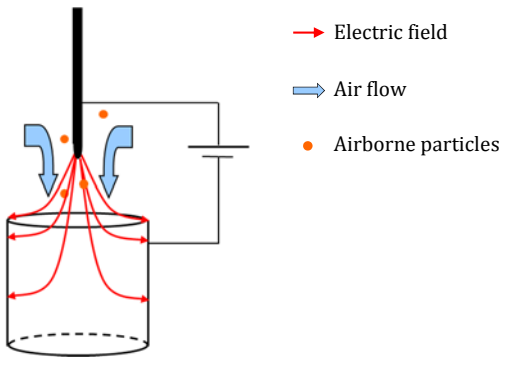

Figure 1: Schematic drawing of an electrostatic precipitator and electroaerodynamic pump based on the design of Quinton et al. [2].

The design of Quinton *et al.* [2] was improved to obtain a device that yields very high collection efficiencies for particles ranging from ten nanometers to several micrometers. It is demonstrated that an efficiency higher than 98% is achievable with a flow rate up to 5 L/min [3]. And this flow rate can be generated without any blower. A prototype was developed from the basic concept to an advanced prototype in order to demonstrate the compactness, autonomy and robustness required for qualifications in the field (see figure 2). The developed prototype is light enough to be worn so as to act as a dosimeter for personal exposure to micron and submicron (bio)aerosols. Also its potential is demonstrated by comparison with traditional sampling methods based on filters.

Figure 2: Evolution of the electrostatic precipitator from a simple experimental device to a robust prototype (from Roux et al. [3]).

Perspectives

Technological developments are now pursued with Bertin Technologies in a joint laboratory. Bertin Technologies has already a range of air samplers dedicated to biocollection (Coriolis® products). The present technology will complement their product range with an ultraportable device capable of collecting a wide range of particles from nanoparticles to microorganisms with a very high efficiency.

Related Publications:
[1] J.-M. Roux, O. Kaspari, R. Heinrich, N. Hanschmann and R. Grunow, "Investigation of a new electrostatic sampler for concentrating biological and non biological aerosol particles", Aerosol Science and Technology, 47:5 (2013) pp. 463-471.
[2] E. Quinton, J.-L. Achard, J.-M. Roux, "Ionic wind generator issued from a liquid filled capillary pin. Application to particles capture", Journal of Electrostatics, 71(6) (2013) pp. 963-969.
[3] J.-M. Roux, R. Sarda-Estève, G. Delapierre, M.-H. Nadal, C. Bossuet and L. Olmedo, "Development of a new portable air sampler based on electrostatic precipitation", Environmental Science and Pollution Research (2015).

A generalization of the Lucas-Washburn-Rideal law to composite microchannels of arbitrary cross-section

Research topic: Capillarity, Open and closed channels, Microfluidics

Authors: J. Berthier, D. Gosselin

Abstract: In this work, we propose a general expression for the determination of the velocities of spontaneous capillary flows in composite, confined microchannels of arbitrary shapes. This expression generalizes the conventional Lucas-Washburn-Rideal model which is valid for cylindrical channels. It is shown that the use of an equivalent hydraulic diameter in the Lucas-Washburn model introduces a bias when the shape of the channel cross-section differs notably from a circle. The approach also shows that relatively large velocities - at the scale of microsystems - can be reached by capillary microflows, depending on the shape of the channel, and that transport distances can be important.

Context and Challenges

Capillary actuation is the preferred solution for moving fluids in point-of-care (POC) and home-care devices. These devices must be portable, robust, user-friendly, low-cost, low energy, and compatible with telemedicine. In capillary-actuated systems, the energy for moving the fluids is embedded in the walls as surface energy.

The dynamics of capillary flows has been developed by researchers in the 1920's (Lucas, Washburn, Rideal and Bosanquet [1,2]. They have derived and verified an expression for the velocity valid for cylindrical channels. This expression has been used since, and extended to channel of arbitrary cross section, by replacing the cylinder radius by the hydraulic radius. We show that this approach is not correct and that it is not the hydraulic radius which should be used but another scale, the average friction length. At the same time, we can calculate the dynamics for open channels, for which no expression was known.

Main Results

We show that, for capillary flows, a scale we have noted "average friction length" is the principal geometrical parameter (Figure 1.A). It indicates the length of wall that the flow really sees.

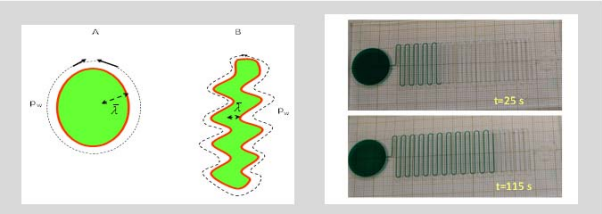

Figure 1: Left: Sketch of the "friction length". Right: View of a capillary flow in an open winding channel (45 cm long).

We demonstrate that its value is given by $\overline{\lambda} = 2 D_H / Po$, where DH is the hydraulic diameter and Po the Poiseuille number. This "friction length" is equal to the hydraulic diameter in the case of cylindrical tubes, but quite different in the case of cross section shapes departing from the circle, such as trapeze or slots. Hence, considerable errors have been done (and even published) by considering only the hydraulic diameter.

In the case of open channels-which are a completely new concept (but useful for space and biomedical applications) no hydraulic diameter can be defined; the calculation is now possible using the "friction length". We have check the approach using different types of channels (Figure 1B).

For usual shapes the friction length can be derived from tables found in the literature [3]. For unusual shapes, it can be either approximated by calculation or by a numerical approach. Dynamics of capillary flows in closed channels of different shapes is shown in Figure 2.

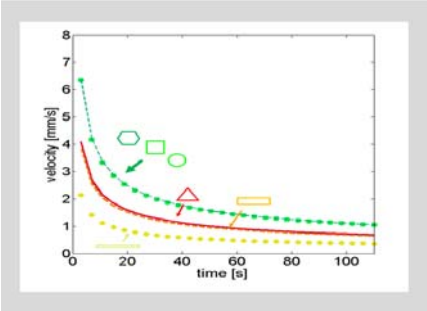

Figure 2: Comparison of the velocity of the capillary flow of water in different channels.

An example of the dynamics of capillary flows in suspended open channels is shown in Figure 3.

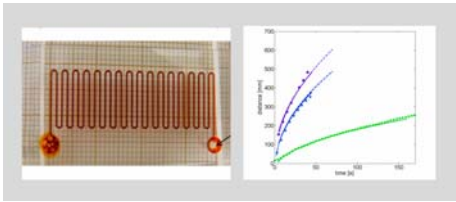

Figure 3: Left: view of the suspended channel; Right: penetration distance with time for different liquids (dots are experimental results, lines are theoretical results).

Perspectives

First, the Lucas-Washburn-Rideal expression is only valid for cylindrical ducts and that the use of an equivalent hydraulic diameter—as is sometimes done in the literature— introduces a systematic bias when the shape of the channel cross-section differs notably from a circle. Second, the notion of friction length gives the possibility to calculate the flow dynamics in complex capillary systems, for example in "flow resistors [4,5].

Related Publications:
[1] R. Lucas, "Ueber das Zeitgesetz des Kapillaren Aufstiegs von Flussigkeiten", Kolloid Z., 23, 15, 1918.
[2] E.W. Washburn, "The dynamics of capillary flow", Phys. Rev., 17, 273-283, 1921.
[3] M. Bahrami, M. M. Yovanovich, J. R. Culham, "A novel solution for pressure drop in singly connected microchannels of arbitrary cross-section", International Journal of Heat and Mass Transfer, 50, 2492–2502, 2007.
[4] R. Safavieh et al., "pre-programmed, self-powered microfluidic circuits built from capillary elements", Lab-Chip, 13, 4180, 2013.
[5] J. Berthier, K. Brakke, E. Berthier, "A general condition for spontaneous capillary flow in uniform cross-section microchannels, Microfluid." Nanofluid. Journal, 16, 779–785, 2014.

Gas chromatography signal processing for pollutant analysis

Research topic: Gas chromatography, Bayesian estimation, Monte Carlo Markov Chain (MCMC)

Authors: F. Bertholon, O. Harant, L. Foan, S. Vignoud, P. Grangeat

Abstract: we describe two methods to estimate the concentration of Polycyclic Aromatic Hydrocarbons (PAHs) in a methanol solution, from a gas chromatography analysis. We present an innovative stochastic forward model based on a molecular random walk. To infer on PAHs concentration profiles, we use two inversion methods. The first one is an Expected A Posteriori (EAP) Bayesian estimation using a MCMC algorithm and Gibbs sampling. The second one is a sparse representation method with non-negativity constraint on the mixture vector. This representation is based on the signal decomposition on a dictionary of chromatographic impulse response functions as defined by the forward model. It is computed using a FOCUSS algorithm.

Context and Challenges

Analysis of mixtures is nowadays essential in pollutant detection and quantification for instance to monitor the air we breathe or the water we drink. Our interest is focused on Polycyclic Aromatic Hydrocarbons (PAHs) in methanol solvent. We are studying methods to infer jointly on the concentration of each PAH and on unknown parameters describing the response function of the chromatographic process. We use a stochastic forward model based on the molecular random walk principle as described by Giddings and Eyring to settle the following signal model:

$$y_i = \sum_{k=1}^{M} c_k P^{GE}(t_i; \theta_k)$$

This model corresponds to a sum of M chromatographic peaks which shape is defined by the Giddings and Eyring's distribution $P^{GE}(t;\ \theta_k)$. The parameters vector θ_k denotes the the kth peak shape parameters and c_k the relative proportions of gas present in the mixture. We need to determine c_k and θ_k from the chromatography signal.

We introduce two methods to invert this model. The first one is an Expected A Posteriori (EAP) Bayesian parameters estimation based on a microscopic model using a Monte Carlo Markov Chain (MCMC) algorithm and Gibbs sampling. We estimate (c_k, θ_k) after drawing a list of N molecular retention times $(\tau_i)_{i=1:N}$ under the time distribution defined by the signal. The second one is a sparse representation method based on a dictionary of macroscopic parametric chromatographic responses $D = \left(P^{GE}(t_i;\theta_j)\right)_{i,j}$. The sparse representation is computed using a FOCal Underdetermined System Solution (FOCUSS) algorithm. We compare those two methods in terms of computational time and quantification performances on experimental data [1].

Main Results

Compared to the sparse representation method the Bayesian estimation needs to know a priori the number of entities present in the mixture. The sparse representation does estimate this number. However, the computing time and the memory space needed for a sparse representation is much more important than for Bayesian inference.

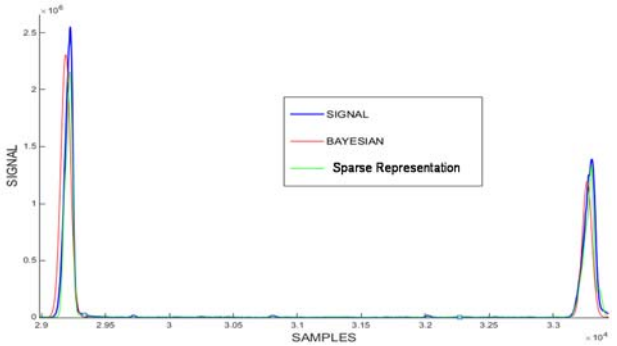

Figure 1: Signal and estimated models for Bayesian and Sparse representation methods.

Perspectives

For the Bayesian approach, we are working on estimation algorithms with an unknown number of peaks. We have introduced non-parametric Bayesian models [2, 3].
The comparison with the 2 methods described here has been presented at the EMBC 2015 conference [4]. We are also studying computing time reduction using variational inference.
For sparse representation on dictionary we propose to reduce the requirement in memory space and to speed the computation by implementing an adaptive dictionary.
The final objective is to combine both approaches in a Bayesian sparse representation algorithm.

Related Publications:
[1] F. Bertholon, O. Harant, L. Foan, S. Vignoud, C. Jutten, P. Grangeat, "Chromatographic signal processing for PAH in Methanol solution", EUSIPCO 2015, 23rd European Signal Processing Conference, Nice, France, 31 th august– 4th September 2015.
[2] O. Harant, L. Foan, F. Bertholon, S. Vignoud, P. Grangeat, "Inférence bayésienne non paramétrique pour l'analyse chromatographique de polluants dans l'eau", XXVème Colloque GRETSI, 8-11 septembre 2011, Lyon, France.
[3] O. Harant, L. Foan, F. Bertholon, S Vignoud., P. Grangeat, "Nonparametric Bayesian inference on environmental waters chromatographic profiles", IEEE International workshop on Machine Learning for Signal Processing (MLSP 2015), Boston, USA, 17th-20th September 2015.
[4] F. Bertholon, O. Harant, L. Foan, S. Vignoud, C. Jutten, P. Grangeat, "From molecular model to sparse representation of chromatographic signal with an unknown number of peaks", EMBC 2015, Proceedings of the 37th Annual International Conference of the IEEE Engineering in Medicine and Biology Society (EMBC 2015), vol. 2015-November, Art. N° 7320211, pp. 7849-7852, Milan, Italy, 25th - 29th August 2015.

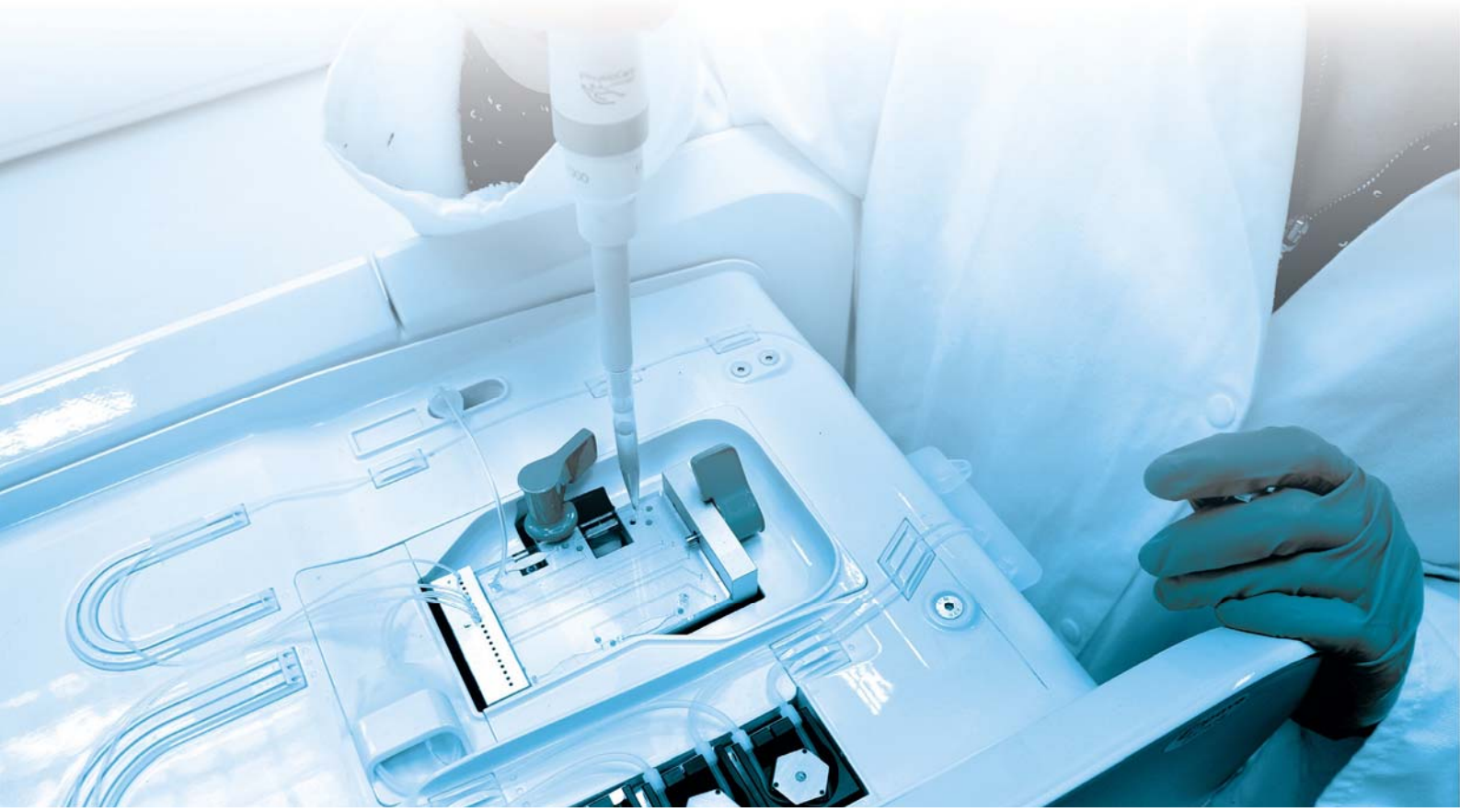

4

WEARABLE DEVICE

- Wireless patch
- Health monitoring at home
- Closed loop therapy
- EEG analysis

Calibration of a wireless patch SpO_2 sensor for respiratory disorders applications

Research topic: Medical optics instrumentation, Blood or tissue constituent monitoring, Spectroscopy

Authors: A. Koenig, R. Gerbelot, C. Desir, P. Jallon, J-M. Dinten

Abstract: Our objective here is to conduct a clinical study in order to calibrate an oximetry sensor on different body locations including wrist (external), forearm (internal), arm (internal), sternum and forehead. This sensor is part of a conformable wireless patch developed for punctual and continuous respiratory disorders monitoring. We confirm with preliminary results of the clinical study that calibration parameters are specific to body location but subject independent, at least for subjects having the same skin phototype. We have demonstrate the possibility to go from a transmittance mode to a reflectance mode thus extending the number of accessible sites for SpO_2 measurements.

Context and Challenges

Pulse oximetry (SpO_2) is a well-known signal recorded for respiratory-related physiological measurements [1]. This non-invasive method measures hemoglobin oxygen saturation in the capillaries. However isolated SpO_2 cannot completely characterize a physiological condition and must be coupled to other measurements such as actigraphy and transcutaneous partial pressure in CO_2 ($PtcCO_2$). In this context, we are pursuing the development of a wireless patch system [2]. On the same wearable and conformable device, actigraphy, SpO_2 and $PtcCO_2$ sensors will be integrated (see Figure 1). The challenge of the SpO_2 sensor development is to go from a classical transmittance mode to a reflectance mode as in the diffuse reflectance spectroscopy technique [3]. Furthermore, the device must be worn on different body sites including wrist, forearm, arm, sternum and forehead and record data during up to 12 hours to allow over night measurements.

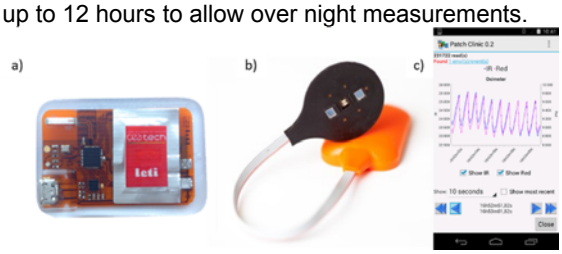

Figure 1: a) Patch, b)SpO_2 sensor and c)smartphone application.

Main Results

The aim of the clinical study is to provide a multi-site calibration of the reflectance SpO_2 sensor. We acquired data on a panel of 18 healthy volunteers. They were exposed to 5 different levels of FiO_2 (Fraction of inspired oxygen) by breathing a hypoxic gas mixture obtained by adding nitrogen to ambient air (ALTITRAINER200®, S.M.TEC, Switzerland). The following SpO_2 targets (±2)% : 98 (nominal state), 90, 85, 80 and 75 define one normoxic condition and four hypoxic conditions to cover the range defined in the norm EN ISO 80601-2-61. These targets were maintained during 3 minutes for physiological parameters to stabilize and controlled by a reference transmittance pulse oximeter. Simultaneously earlobe arterialized blood sampling (heparinated 140 µL micro-tubes) was performed to measure arterialized SaO_2 (hemoglobin oxygen saturation) with RapidLab 1265-Siemens®. See Figure 2.

Two patch devices were used. One was systematically placed on the forehead for almost all subjects; the other was placed either on wrist, forearm, arm or plexus. Thus, 14 measurements were done for the forehead site, 8 for the wrist and sternum and 4 for each of the other sites.

Figure 2: Patch measurement on forehead and wrist, blood sampling at earlobe.

Data analysis matching the SaO_2 values obtained on the arterialized blood and the non-calibrated SpO_2 patch sensor data has shown the need for a site dependent calibration curve. After calibration, the SpO_2 patch sensor shows a good accuracy root mean square (Arms) in agreement with the norm (must be less than 4% in 70%-100% range) (see Figure 3).

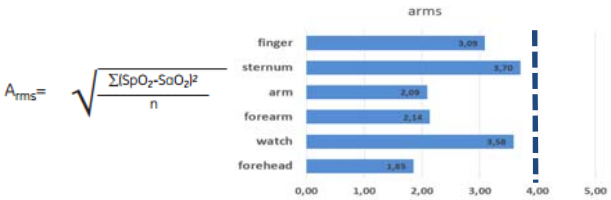

Figure 3: Accuracy root mean square < 4%.

This work is done in collaboration with Agir à Dom, HP2 Lab at Univ. Grenoble Alpes, UM Sports Pathologie at Hôpital Sud Grenoble and U1042, INSERM. This work was supported by the French National Research Agency (ANR) through Carnot funding.

Perspectives

We confirm with these results that calibration parameters are specific to body location but subject independent, at least for subjects having the same skin phototype. We can measure SpO_2 in a reflectance mode with the patch on several locations, forehead and wrist being easier than the other sites.

Related Publications:
[1] D. Desir, M. Doron, J.-C. Borel, C. Loïodice, M. Lesgoirres, R. Guillemaud and J. L. Pepin, “Le seuil optimal pour détecter un micro-éveil par l’écrasement de l’onde de pouls est différent entre sujets sains et patients SAOS". Médecine du Sommeil, 12(1), 23 (2015).
[2] R. Gerbelot, A. Koenig, C. Goyer, J. Willemin, C. Désir, J. Porcherot, H. S. Kane, R. Guillemaud, J.-C. Borel and P. Jallon, “A wireless patch for sleep respiratory disorders applications”, EMBC Milan, (2015).
[3] A. Koenig, S. Grande, K. Dahel, A. Planat-Chrétien, V. Poher, C. Goujon, J-M. Dinten, “Diffuse reflectance spectroscopy: a clinical study of tuberculin skin tests reading”, BiOS, 2 - 7 February 2013, San Francisco, California USA.

Sleep arousals detection against photoplethysmography signals for monitoring sleep fragmentation and sleep disorders

Research topic: eHealth, Health monitoring at home, Sleep monitoring, Unsupervised processing

Authors: L. Gerfault, C. Desir

Abstract: Our goal is to assess Sleep quality by cheaper, more comfortable mean, with at home monitoring capacity. Sleep quality can be assessed by the amount of sleep arousals. These lasts are taking part of regulation of sleep process but are also marker of sleep disruption. They are measured by EEG means during Polysomnography exam, a one-shot, expensive, time consuming procedure. To demonstrate that continuous sleep monitoring at home is achievable, we have developed automatic detection using optical measurements of blood pulse wave. We obtain 85% sensitivity and 83% specificity at detecting sleep arousals for 52 patients.

Context and Challenges

Sleep arousals are manifestations of autonomous nervous system (ANS). They are related to various sleep disorders like obstructive Sleep Apnea syndrome (OSA) and restless leg syndrome. They have been introduced as the 'gold standard' to detect sleep fragmentation, a factor contributing to impaired daytime function and sleepiness. The standard method to detect sleep arousals is EEG measurements, and for sleep monitoring they are associated to other physiological measurements in an exam called Polysomnography (PSG).

PSG is a one-shot, expensive, time consuming and painful procedure, moreover in a foreign environment for the patient with long waiting list due to limited availability. There is a strong need for clinically validated tools providing aided diagnosis, that are cheaper, more comfortable than PSG with at home monitoring capacity and continuous screening (long term or longitudinal testing).
In parallel with the development of a conformable wireless patch, we developed algorithms to assess health monitoring against the physiological parameters measured by this patch.

Thus, Sleep Arousals detection is an adequate target as associated signaling is found in blood pulse wave and can be measured by optical peripheral sensor (Photoplethysmography i.e. PPG).

Our approach consists in:

- the extraction of relevant features from single PPG signal,
- the local detection of individual sleep arousals events using classification algorithm (Random Forest) based on the extracted features,
- the computation of indexes for the quantification of the patient state for real-time, continuous and longitudinal monitoring,
- the possibility to estimate the patient state (e.g. healthy or pathological).

Main Results

The database (52 subjects: healthy, apneic, insomniac, restless leg syndrome) was acquired by home-based or in-lab full-night PSG (Sleep Laboratory Grenoble University Hospital).

In this database, PPG Infra-Red signal was measured at finger location by clinical device. Finger sensor is in these case a proxy of blood pulse wave monitoring which can be measured by our patch in various body location.
Sleep characteristics (arousals, sleep disorders …) were scored manually according to standard criteria. 5194 arousals were annotated.

About 40 000 windows of 60s duration were extracted and considered for classification (half with sleep arousal, half without (no event)).

	Detected by algorithm	
Annotated	no event	sleep arousal
no event	0.83	0.15
sleep arousal	0.17	0.85

Figure 1: Confusion matrix for automatic sleep arousal detection.

The preceding confusion matrix shows that 85% of the considered windows containing sleep arousals are correctly classified. A good specificity of 83% is also obtained with an adequate classification of no event windows.
These spo2ures have to be evaluated against inter-scorer agreement. The closest available figures upon scoring against EEG signals are from sleep stages scoring [1]. Sleep stage agreement averaged to 82.6%.

Perspectives

In this study, we have shown the ability to obtain a good accuracy in the detection of sleep arousals using optical peripheral sensor for multiple subjects in different conditions during one night.
A continuous sleep monitoring is achievable due to the use of light device and automatic detection.
The level of performance compared to gold standard is acceptable for this kind of application.
The result obtained – possible to measure sleep arousal with non invasive devices - makes possible to have new insights and new ways to manage this kind of diseases.

Related Publications:
[1] R. S. Rosenberg and S. Van Hout, Steven, 2013. "The American Academy of Sleep Medicine Inter-Scorer Reliability Program: Sleep Stage Scoring", Journal of Clinical Sleep Medicine : JCSM : Official Publication of the American Academy of Sleep Medicine 9 (1): 81–87. doi:10.5664/jcsm.2350
[2] C. Desir, L. Gerfault, J.C. Borel, C. Loïodice, M. Lesgoirres, R. Gerbelot, J.-L. Pépin, "Système expert supervisé pour la détection de micro-éveils autonomiques", Congrès du Sommeil 2015, Nantes.

The french artificial pancreas Diabeloop clinical trials: 1-day-bioregulation in medical premises

Research topic: Diabetes, Insulin therapy, Closed loop

Authors: E. Amat, M. Antonakios, M. Doron, C. Franco, R. Guillemaud, P. Jallon, S. Lachal, J. Porcherot

Abstract: The Artificial Pancreas objective is to optimize the rate of insulin delivery for Type 1 diabetic subjects. Over 180 000 people in France are subject to this chronic disease, which is a daily burden in terms of glycaemic control. Most frequent treatment issues are hypoglycemia and hyperglycemia, causing lack of adherence to glycaemic objectives. The bio-regulation implemented in Diabeloop is based on a Model-Predictive-Control (MPC). Significant improvement both in the algorithm and the system were performed since the beginning of the project in 2011. In 2014-2015, the clinical trials began with the bio-regulating algorithm operational during 24 hours in a medical context.

Context and Challenges

The Type 1 diabetes treatment is based on daily injections of insulin. The state-of-the-art treatment is set up on functional insulinotherapy based on carbohydrate counting, insulin boluses associated with meals and estimation of the daily insulin basal rates for physiological needs unrelated to meals. Despite large improvements in the glycaemic control, there are still numerous issues due to hypoglycemia (short-term effects) and hyperglycemia (long-term comorbidities).

Half of the French subjects with glycaemic control leads them to comorbidities. The improvement of the temporal pattern of insulin delivery should improve the medical conditions of the bio-regulated diabetic people.

To address this issue, the concept of the artificial pancreas was developed. The four components of the systems are

- a Continuous Glucose Monitor (CGM) which measures the interstitial glycaemia with a 5-minute-frequency,
- an insulin pump which delivers insulin both with a predefined 24-hour-delivery-scheme (the basal rate) and user-defined boluses of insulin (tailored to meal size)
- a user interface allowing the medical team to provide the usual treatment of the patient and allowing the patient to inform the algorithm with the time and size of her (his) meals
- a smartphone being the communication platform between the CGM, the pump, the user and the computation platform for the algorithm. Eventually, it could also be used for the remote monitoring of the system.

Main Results

Previous clinical experiments, performed in 2013 in hospital setting, had a duration of 1 day [1]. In 2014-2015, significant improvements were implemented both in the system and in the algorithm, allowing clinical trials lasting 24h in medical premises for 15 subjects. The bioregulation results in terms of CGM glycemia are compared to the CGM results obtained with the patient's usual treatment.

The Type 1 diabetic model is based on Hovorka model (2002). The personalization of the model objective is to take into account the unique physiology of each patient [2].

This issue is performed with advanced techniques with the recorded data in meals and insulin delivery. Predicted glycaemic trajectories are then used to optimize the insulin basal rate in the future.

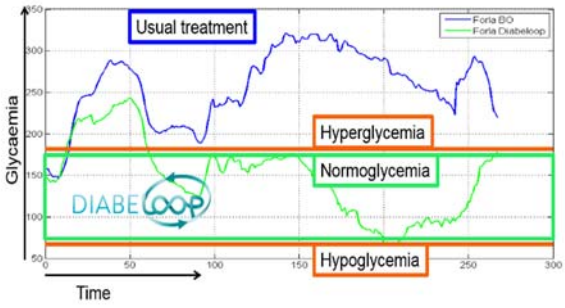

Figure 1: Results obtained with an inpatient in CERITD. The x-axis represents 24 hours. The y-axis is the glycemia observed CGM (in mg/dl), in blue for the usual treatment and in green when the bioregulation is used. Normoglycaemia is represented within the green box, while hypoglycaemia and hyperglycaemia are below and above the orange lines.

The Diabeloop algorithm was tested in 3 hospitals on 15 patients. Overall glucose control was similar during both sessions with percent time in 70-180 mg/dl range of 66.0±20.8 (bioregulation) vs. 59.1±21.8% (usual treatment) and mean blood glucose level of 151±27 vs. 141±43 mg/dl, respectively. Interestingly, percent time < 70 mg/dl was reduced during bioregulation: 3.9±3.7 vs. 13.5±13.6%, more specifically from 23:00 to 07:00: 0.0±0.2 vs. 21.6±27.8% (p=0.0002). Number of patients with at least one event <70mg/dl from 23:00 to 07:00 was 1/14 vs. 8/14 (p= 0.0065).

Perspectives

Improvements in the algorithm were implemented during 2015. New clinical trials are ongoing since late 2015 for a sedentary context (15 subjects, 3 hospitals). They show good performances. Next clinical trials will focus on either large meals or physical activity periods. Those two patterns are very challenging for the control of normoglycaemia. Outpatient setting will then be considered.

Related Publications

[1] M.-A. Quemerais, M. Doron, F. Dutrech, V. Melki, S. Franc, M. Antonakios, G. Charpentier, H. Hanaire, PY. Benhamou, Diabeloop Consortium, "Preliminary evaluation of a new semi-closed loop insulin therapy system over the prandial period in adult patients with type 1 diabetes: the WP6.0 Diabeloop study", Journal of Diabetes Science and Technology, 2014.

[2] E. Renard, P.-Y. Benhamou, S. Franc, A. Farret, S. Lablanche, I. Xhaard, J. Place, M. Antonakios, P. Jallon, G. Charpentier, "Multicentre assessment of usability and safety of a model-predictive control algorithm with enhanced hypoglycemia minimizer for closed-loop insulin delivery in patients with type 1 diabetes: a randomized control cross-over inpatient clinical trial", Diabetes Technology Meeting, 22/10/2015 - 24/10/2015, Bethesda, Maryland, USA.

Mental workload estimation based on personalized multi-electrodes EEG system

Research topic: Electroencephalography- Mental State Monitoring

Authors: S. Bonnet, R. Roy

Abstract: Mental workload estimation is of crucial interest for user adaptive interfaces and neuroergonomics. Its estimation can be performed using event-related potentials (ERPs) extracted from EEG recordings. Several ERP spatial filtering methods have been designed to enhance relevant EEG activity for active brain-computer interfaces. However, to our knowledge, they have not yet been used and compared for mental state monitoring purposes. Different methods are compared in their performance to allow an accurate classification of mental workload.

Context and Challenges

Mental state monitoring (MSM) can be performed accurately by using electroencephalography (EEG). Workload is a mental state that has recently been reconsidered in the neuroergonomics area. This mental state is particularly relevant for implementing user adaptive interfaces and user monitoring devices for safe transportation. The regain of interest comes from the enormous progress in the technological side and the processing side. Challenges concern the use of dry electrodes, the amplification electronics with low-voltage signals, interferences and finally the real-time signal processing. Event-related potentials (ERPs) are electrical deflections (positive or negative) observed within scalp EEG data in response to the appearance of a given stimulus. This activity is a well-known marker of cognitive functions such as working memory load. Manipulating memory load (e.g. number of items to keep in memory) is a way to modulate task difficulty, or more generally mental workload. This paper deals with spatial filtering methods applied on the ERPs to enhance them [1, 2]. In the present study, we compare the usefulness of different spatial filtering methods for ERP-based mental workload estimation. The goal is to classify situations where the workload is high versus low.

Main Results

An experiment has been designed to manipulate workload using a modified Sternberg paradigm (N=20 subjects). The participants had to memorize a list of sequential digits (either 2 or 6) visually presented on a computer screen. Then a probe item flanked with question marks was presented and the participant had to answer whether it was present or not in the previous list using a response box. This research was promoted by the University Hospital of Grenoble, approved by the local French ethics committee (ID: 2012-A00826-37) and the French health safety agency (B120921-30). 32 EEG channels were recorded during the experiment. The EEG dataset $\mathbf{X} \in \mathbb{R}^{N_e \times N_t}$ was first band-pass filtered 1-40Hz, spatially filtered $\mathbf{Z} = \mathbf{w}^{\mathrm{T}}\mathbf{X}$ and finally epoched (600ms) with respect to the appearance of the probe item. The spatial filter with two virtual channels is either based on principal component analysis (PCA), canonical correlation analysis (CCA) and xDAWN algorithm. The raw condition extracts the EEG signals from electrodes Cz and POz. Finally, a Linear Discriminant Analysis (FLDA) intra-subject classification step was performed, using a shrinkage estimation of the covariance matrices. The grand average ERP at the Cz location is shown in Figure 1. When workload is increased, a significant decrease in amplitude occurs at the group level for the N2 component *($p < .05$)*.

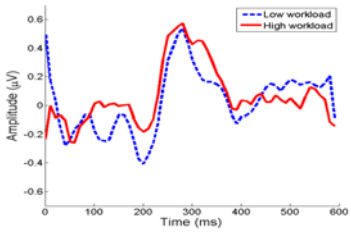

Figure 1: Grand average ERP at the Cz electrode (across all participants).

The classification performance results are given in Figure 2. Classification performance was significantly different from chance level only when a spatial filtering step is used ($p < 0.001$). Moreover, classification performance was significantly different between the four chains. Both xDAWN (97%) and CCA (98%) gave significantly better results than PCA (88%), and all the chains that included a spatial filtering step gave significantly higher results than the RAW chain ($p<0.001$). There was no significant difference in performance between the CCA and the xDAWN chains ($p = 0.99$).

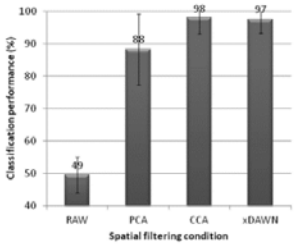

Figure 2: Classification accuracy depending on the spatial filtering method.

Perspectives

The optimal performances we obtained in a single-trial fashion, indicate that workload estimation using evoked potentials is more than feasible and should be considered for MSM system implementation. Future work should evaluate the use of task-independent stimuli, and even ignored stimuli, such as ignored auditory probes. The use of such probes would be less intrusive and would allow for a quick although non continuous mental state assessment.

Related Publications:
[1] R. N. Roy, S. Bonnet, S. Charbonnier, P. Jallon, A. Campagne, “A comparison of ERP spatial filtering methods for optimal mental workload estimation”, 37th Annual Intl. Conf. of the IEEE Engineering in Medicine and Biology Society (EMBC-2015), Milano, Italy, August 25 – 29, 2015. pp. 7254-7257.
[2] R. N. Roy, S. Bonnet, S. Charbonnier, A. Campagne, “Enhancing Single-Trial Mental Workload Estimation through xDAWN Spatial Filtering”, 7th International IEEE EMBS Conference on Neural Engineering NER-2015, April 22-24, Montpellier, France, pp 360-363.

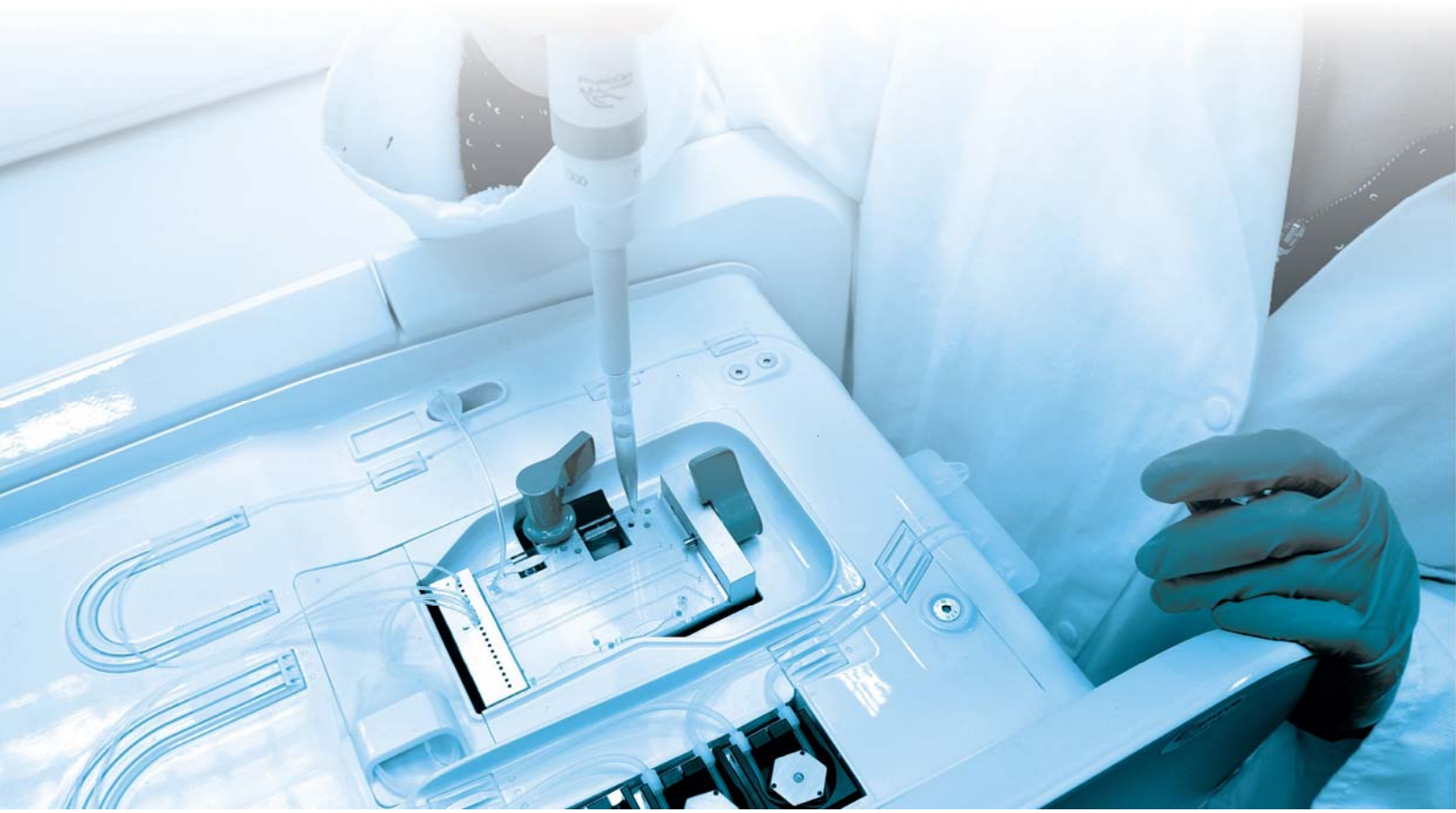

5

IMPLANTABLE DEVICE

- Selective recording & stimulation
- Electrical impedance tomography
- Brain computer interface
- NIR implant

Selective recording and stimulation in vagus nerve stimulation applications

Research topic: Microelectrode, Cuff, Reliability, Neural, Stimulation and recording recording, Iridium oxide

Authors: S. Maubert, S. Bonnet, F. Bottausci, F. Baleras, S. Gharbi, A. Bourgerette, G. Grenot, C. Pudda, F. Sauter

Abstract: This paper describes the design, the fabrication and the experimental results of flexible multi contact cuff electrode for interfacing, for neural recording and for stimulation. The contact impedance must be as low as possible to increase the signal to noise ratio and the injection charge of the active material as high as possible to enhance long term stability. Iridium oxide exhibits lower impedance, and also high charge injection. A process was developed for fulfilling these requirements. We have demonstrated the selectivity for the stimulation on animal model for the cardiac activities, and the contribution of the neural sensing as new biomarker.

Context and Challenges

The electrode is a key component; it allows measuring the bioelectrical signal from the nerve or applying the current to the nerve. The trend in neural electrical stimulation is towards system having a higher number of electrodes for high spatial resolution and consequently improving the selectivity. An important advantage of the microelectrode is the ability to stimulate a comparatively small volume of neural tissue and to record the action potential from small population of fibers. Another important aspect concerns contact impedance that must be as low as possible to increase the signal to noise ratio. Indeed the objective is to extract the nerve activity in the range of few microvolts and reject noise (artifacts from EMG, ECG, in the range of microvolts). For reliable active contact for stimulation, the active material has to demonstrate high charge injection properties, to ensure safe and long lasting device. The iridium oxide fulfills the requirements in term of low impedance, and high charge injection.

Main Results

A deposition process was developed for the sputtered iridium oxide for fulfilling these requirements of impedance and high charge injection. We obtained a Cathodic Storage Capacity (material capacity to store charges, therefore available for being injected in the tissue) about 13 mC/cm^2. The parylene-based electrode with platinum coated with oxide iridium was fabricated. The packaging of the flexible microelectrodes is also challenging. Indeed for multi-contact electrodes, multiple wires must be connected to thin and small electrodes. A cuff with a good seal allows an efficient stimulation by confining the stimulation current to the inner space of the electrode and avoiding the current leak, and the contamination of other tissues around. A polyester surgical mesh is first coated with a layer of implantable silicone. The parylene-based electrodes are reported on the reticulated coated mesh using the silicone by a screen printing technology. The cuff is shaped on a cylinder. Test structures were specifically designed for performance evaluation. A specific test bench was developed for the mechanical cycling and for evaluating the mechanical robustness of the thin film devices. All the test structures evaluated have successfully shown no significant effects of the bending of the metal lines. The resistance stayed the same after 600 to 1000 bending cycles around a 3 mm and 1 mm cylinder.

We investigate the simultaneous use of two separate multi contact cuff electrode for recording and for peripheral selective nerve stimulation in pig experiments. The goal is to perform selective vagus nerve stimulation (VNS) by using spatio temporal patterns and thus minimize the side effects. The nerve activity is quantified by analysis of compound action potential (CAPs) that are evoked by the different VNS configurations whereas ECG analysis is done by studying heart rate variability during VNS.
The microelectrodes were able to selectively evoke neural activities and physiological modifications. A surrogate measure of autonomic activity, such as heart rate changes, was observed for particular vagus nerve spatial configuration. Different CAPs have also been recorded on the different contacts placed around the periphery of the vagus nerve.

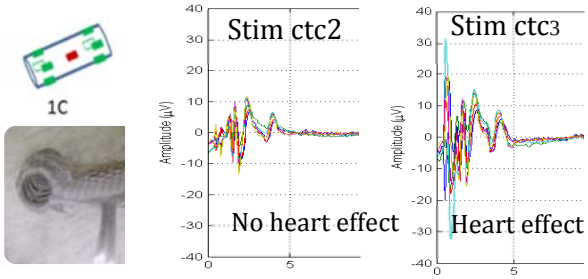

Figure 1: Left VNS-stimulation configuration. Anode electrodes are shown in red, cathodes in green, and multielectrode cuff
Right: Evoked CAPs for the two different contacts for 1C configuration.

This work was partly supported by Bpifrance within the “Investment for the Future” program in France.

Perspectives

The multicontact electrodes that we have developed exhibits a promising *in vitro* reliability. We plan to evaluate our technology for an implantation of several weeks in animal model. Multicontact electrodes are well indicated to recruit specific fibers in a topographical way and also to record regional fiber activity. The sensing of the neural activity is an interesting biomarker to optimize the therapy for nerve stimulation medical applications and open new perspectives for the system control by a close loop with this new input.

Related Publications:
[1] S. Maubert, S. Bonnet, F. Bottausci, F. Baleras, S. Gharbi, A. Bourgerette, G. Grenot, C. Pudda, F. Sauter, C. Gallet, J.-L. Divoux, C. Henry, "Selective recording and stimulation in Vagus Nerve Stimulation applications”, GDR 2904, Multielectrode Systemes for Neurosciences, Jan 2016.
[2] S. Bonnet, A. Bourgerette, S. Gharbi, F. Baleras, F. Bottausci, N. Torres-Martinez, C. Cretallaz, F. Sauter-Starace, C.-H. Malbert, L. Laporte, C. Gallet, A.I. Hernandez, G. Carrault, O. Rossel, D. Guiraud, J.-L. Divoux, C. Henry, S. Maubert, “Cardiac and neural analysis for VNS applications”, IEEE NER 2015.

Peripheral nerve electrical impedance tomography (EIT)

Research topic: Electrical impedance tomography, Image reconstruction

Authors: A. Fouchard, S. Bonnet, L. Hervé

Abstract: Medical electrical stimulators adapted to peripheral nerves make use of multicontact cuff electrodes (MCC). Intended until now for stimulation or recording, MCC can also be used as a means of transduction to characterize the nerve by impedancemetry. The objective of this long-term project is to determine the feasibility of obtaining information on the electrical property distribution of a nerve section, by electrical impedance tomography (EIT) using microelectrode arrays.

Context and Challenges

A peripheral nerve can be electrically stimulated by placing a cuff electrode around it and by injecting electrical currents between two contact electrodes. Spatial selectivity can be achieved by employing multi-contact cuff electrodes and complex spatio-temporal patterns. Moreover it is also possible to record neural activity from the nerve using the same type of electrodes. Electroneurography (ENG) is employed to assess conduction velocity and to quantify the type/size of recruited fibers. Such recording/stimulation device can be built on distinct/same cuff electrode. These new technological developments open the way for *in vivo* electrical impedance tomography (EIT) that aims at reconstructing conductivity spatial distribution inside a medium from electrical recordings on its boundary. So we aim at creating an *in vivo* EIT system using a mixed apparatus between ENG and neuromodulation. To achieve such long-term goal, implementation of efficient methods to handle calculations is a key issue to address 3D electrical property reconstructions. Using a finite volume element method, we develop a nodal framework for handling both the forward problem and the sensitivity analysis.

Main Results

The design and implementation of numerical solvers is an active area of research of EIT, since its weak formulation is uncommon. To tackle the forward problem and derive sensitivity-based reconstruction schemes, the finite element method (FEM) is currently the standard method, along with an elemental discretization of conductivity. While calculation parallelization and deduction of nodal Jacobian offer ways to enhance calculus efficiency, we propose an alternative framework that lowers the required computational resources. It allows both to guarantee the local conservation of the current-density involved in sensitivity computations, and to directly compute a Jacobian matrix that scales with the number of nodes rather than the number of elements.

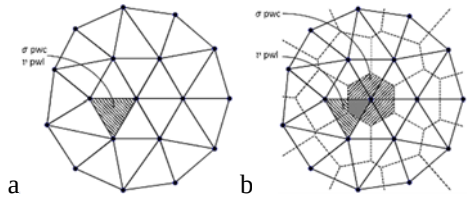

Figure 1: Assumptions for the EIT nodal framework; a. FEM standard case; b. FVE case.

The approximation of the complete electrode model for EIT is derived under the FVE workflow, and leads to the determination of an admittance sparse symmetric matrix $\mathbf{Y} \in \mathbb{R}^{(N_n+E)\times(N_n+E)}$.

Internal and electrode potentials can thus be predicted. This approach has already been applied with success to the diffuse optical tomography (DOT) image reconstruction problem. The sensitivity analysis is further processed following a perturbation approach.

One-step differential reconstructions were obtained from a saline phantom, featuring 14 equally-spaced copper electrodes. Inclusions were simulated using metallic cylinders of either 1/8 or 1/4 of the phantom diameter (Figure 2).

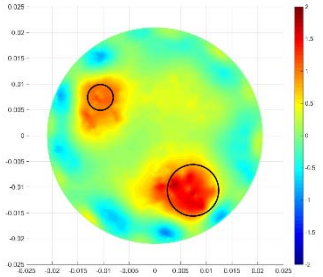

Figure 2: 2D time difference FVE reconstruction from experimental data, with estimated 5% noise.

Perspectives

The proposed approach allows reducing the computational requirements for parameter estimation. The proposed workflow is tested successfully against experimental data. It makes it possible to define complex geometries, as in the nerve, and still perform forward computations in a reasonable time. It is a mandatory aspect of EIT image reconstruction for nerve imaging. Further investigation might take advantage of its lower computational resource requirements to perform large-scale multispectral imaging. Preliminary EIT recordings have been done at the GIN facility during acute experiments on rodents and impedance changes have been observed on a single 4-point electrode impedance measurement. This impedance change is reminiscent of the local depolarization of the membrane that occurs during action potential propagation. This seems to indicate that by synchronizing evoked activity and EIT recording, we may be able to determine conductivity change in time.

Related Publications:
[1] A. Fouchard, S. Bonnet, L. Hervé, O. David, (2015) "A current-density conservative nodal framework for EIT", Proceedings of the 16th International Conference on Biomedical Applications, Electrical Impedance Tomography, Neuchâtel, Switzerland, June 3-5, 2015.
[2] A. Fouchard, S. Bonnet, L. Hervé, O. David, (2015), "Flexible Numerical Platform for Electrical Impedance Tomography", COMSOL conference, October 14-16, 2015.

A Brain Computer Interface human platform to control a 4-limb exoskeleton based on the ECoG-recording implant WIMAGINE®: toward a clinical trial

Research topic: Neurosciences, Innovative implantable medical device

Authors: A.-L. Benabid, C. Mestais, G. Charvet, F. Sauter-Starace, M. Foerster, D. Ratel, T. Aksenova, A. Verney

Abstract: We are currently conducting a project to develop an innovative Brain Computer Interface (BCI) platform to allow a quadriplegic subject recovering partial mobility using effectors such as a 4-limb exoskeleton. Movements imagined by the subject induce electrical activity in his motor cortex which is recorded by a wireless and fully implantable medical device, called WIMAGINE® to record ElectroCorticoGrams (ECoG). These signals are processed in real time by BCI algorithms to control effectors after a training period. Authorizations to start the clinical trial at Clinatec® were obtained in December 2015 from French regulatory agencies.

Context and Challenges

The goal of Clinatec® Brain Computer Interface Project is to provide the proof of concept that it is possible to control complex effectors, such as a 4-limb exoskeleton, thanks to brain activity monitoring and decoding to open new opportunities to motor disabled, in particular for tetraplegic subjects. Thanks to a wireless 64-channel ECoG (ElectroCorticoGram) recording implant for chronic use named WIMAGINE® [1] and an innovative signal processing, the subject should be able to control a 4-limb exoskeleton EMY (Enhancing MobilitY) [2].

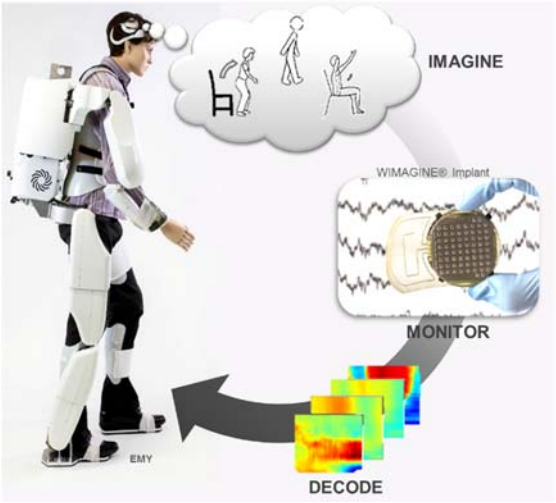

Main Results

ECoG signals from the subject's brain are recorded and wirelessly transmitted to a base station by the WIMAGINE® implant. This implant is composed of an array of 64 biocompatible electrodes, a hermetic titanium case which houses electronic boards, biocompatible antennas for wireless transmission of the data, and a remote power supply. The design of the WIMAGINE® implant takes into account all the constraints for active implantable medical devices 93/42/CEE and 90/385/EEC. For this purpose, our team designed and handled the implant manufacturing according to ISO 13485, as well as qualification tests according to the European directive 2007/47/EC and ISO standards (risk analysis ISO 14971, ISO 45502 for implantable devices electrical and mechanical safety, and EN 60601-1 for electrical safety and electromagnetic compatibility of the external unit). Long-term biocompatibility abides the ISO 10993 requirements, in particular the local tolerance and systemic effects after 26 weeks contact duration in animals.

Innovative ECoG signal decoding algorithms allow self-paced control of the exoskeleton, and will facilitate decoding the subject's brain activity [3, 4]. The neuronal signal processing approach is based on a tensor data analysis. It allows simultaneous treatment of the signal in several domains, frequency, temporal, and spatial.

Before applying the BCI platform to patients, a set of preclinical experiments were carried out on male Macaque Rhesus. Ethical approval was obtained from ComEth in accordance with the European Communities Council Directive of 1986 (86/609/EEC) for care of laboratory animals. High performance decoding of the continuous three-dimensional hand trajectory from epidural ECoG signals of the primate's brain allows reproducing the arm movement by the exoskeleton arm (EMY) in real time. To ensure future clinical applications, algorithms were also tested in control human subjects, in noninvasive MEG acquisition system while they are executing real or imagined hand movements. Both real and imagined hand movements were successfully decoded from the recording of 36 MEG sensors facing the sensorimotor area. Initial results yield an average Pearson Correlation (PC) between decoded and the tracked/intended movements of 0.55±0.14 for 3D free real movements, and of 0.38±0.10 for 3D cued-paced imagined movements (3 coordinates, 2 sessions per paradigm, 2 subjects), which is very encouraging.

Perspectives

The 5-year clinical research protocol "BCI and Tetraplegia" was approved in December 2015 by French authorities (ANSM) and ethical committees. Professor Benabid as Principal Investigator will include 5 tetraplegic patients at Clinatec. This trial will allow testing and refining algorithm paradigms, evaluating the exoskeleton usability in a controlled environment, and benefiting from patient feedback to design a range of solutions to be used at home.

Related Publications:
[1] C. Mestais, G. Charvet, F. Sauter-Starace, M. Foerster, D. Ratel, and A.-L. Benabid, "WIMAGINE: Wireless 64-Channel ECoG Recording Implant for Long Term Clinical Applications", IEEE Transactions on Neural Systems and Rehabilitation Engineering, Jan. 2015.
[2] Y. Perrot, A. Verney, B. Morinière, and P. Garrec, "EMY: Full-body Exoskeleton", ACM SIGGRAPH Emerging Technologies, Anaheim, USA, 2013.
[3] A. Eliseyev and T. Aksenova, "Stable and artifact-resistant decoding of 3D hand trajectories from ECoG signals using the generalized additive model", J. Neural Eng. 11 (2014) 066005 (13pp).
[4] A. Eliseyev and T. Aksenova, "Recursive N-way partial least squares for brain-computer interface", PLoS One, vol. 8, p. e69962, 2013.

Preclinical proof of concept of neuroprotection induced by intracerebral near infra-red illumination in Parkinson's disease

Research topic: Parkinson's disease, Infrared light, Neuroprotection, Active implantable medical device

Authors: C. Moro, C. Chabrol, A.-L. Benabid

Abstract: There is no curative therapeutic strategy for Parkinson disease (PD) nowadays, but only symptomatic ones. On a non-human primates preclinical model of PD, we demonstrated for the first time a neuroprotective effect of intracerebral near infra-red illumination, allowed thanks to the development of a chronic cerebral implant developed at Clinatec. Dopaminergic neurons of substancia nigra pars compacta (which degenerate in PD and induce symptoms) were protected. Behavior of animal was significantly preserved. These results are very promising for a new therapeutic strategy for patients.

Context and Challenges

Parkinson's disease (PD) is a slow and progressive movement disorder. Motor disorders manifest as a consequence of degeneration of dopaminergic neurons in the substantia nigra pars compacta (SNc) of the basal ganglia. The current treatment option for most patients with PD is dopamine replacement drug therapy, followed by surgery in selected patients. The basic strategy of each treatment is simple: dopamine drug therapy aims to replace the dopamine lost from the system, while surgery aims to correct the abnormal function of the basal ganglia circuitry caused by the loss of the dopamine. The surgical option is usually recommended to patients after the efficacy of drug treatment lessens or when the disease has progressed significantly. Both of these main treatments provide symptomatic relief. Current "gold standard" treatments for PD are effective at attenuating motor signs, but they do not reliably slow disease progression. Thus, the discovery of neuroprotective approaches is essential.

Recent data illustrate a real potential for the development of near infrared light (NIR) therapy as a putative neuroprotective strategy. NIR treatment has been reported to reduce cell death, increase adenosine triphosphate content, and decrease levels of oxidative stress among cultured cells after exposure to parkinsonian toxins. Furthermore, NIR offers neuroprotection to dopaminergic cells in the well-known 1-methyl-4-phenyl-1,2,3,6-tetrahydropyridine (MPTP) mouse model and in the K369I transgenic mouse model, which also shows a progressive degeneration of nigral dopaminergic cells.

Main Results

To examine whether NIR treatment reduces clinical signs or offers neuroprotection, a light-delivering device was developed at Clinatec for preclinical use. Optical fiber device delivering NIR light was chronically implanted bilaterally into parkinsonian non-human primates (NHP) brain close to the SNc. MPTP injections were made over a 5- to 7-day period, during which time the NIR device was turned on. This was then followed by a 3-week survival period.

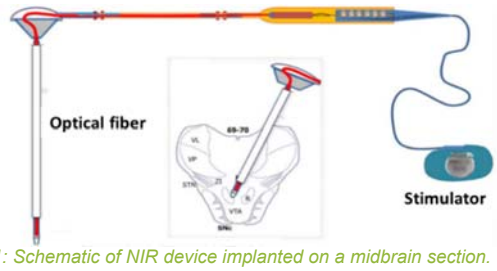

Figure 1: Schematic of NIR device implanted on a midbrain section.

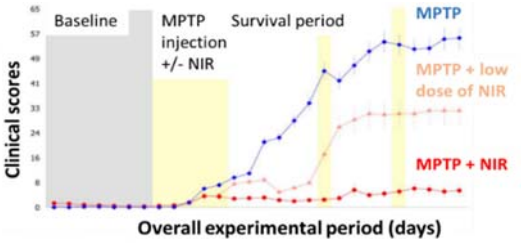

Figure 2: Clinical evaluation.

NHPs were evaluated clinically and behaviorally, and their brains were processed for immunohistochemistry.

NHP in the MPTP group developed severe clinical and behavioral impairment. By contrast, the MPTP-NIR group developed much less clinical and behavioral impairment; some NHP developed moderate clinical signs because of limited NIR exposure, whereas the majority developed few clinical signs. NIR was not toxic to brain tissue and offered neuroprotection to dopaminergic cells and their terminations against MPTP insult, particularly in animals that developed few clinical signs. Altogether NIR exposure preserves dopaminergic survival, corrects the abnormal neuronal activity generated by MPTP, as well as improves locomotor activity [1].

Perspectives

Results of these experiments open the door to a new therapeutic field, holding great hopes for neurodegenerative processes treatment. Our findings create the template for translation into clinical trials. We are currently developing an implantable prototype device for chronic use to be evaluated on a clinical trial in PD.

Related Publication:
[1] Darlot and Moro, Annals Neurology 2016 Jan;79(1):59-75

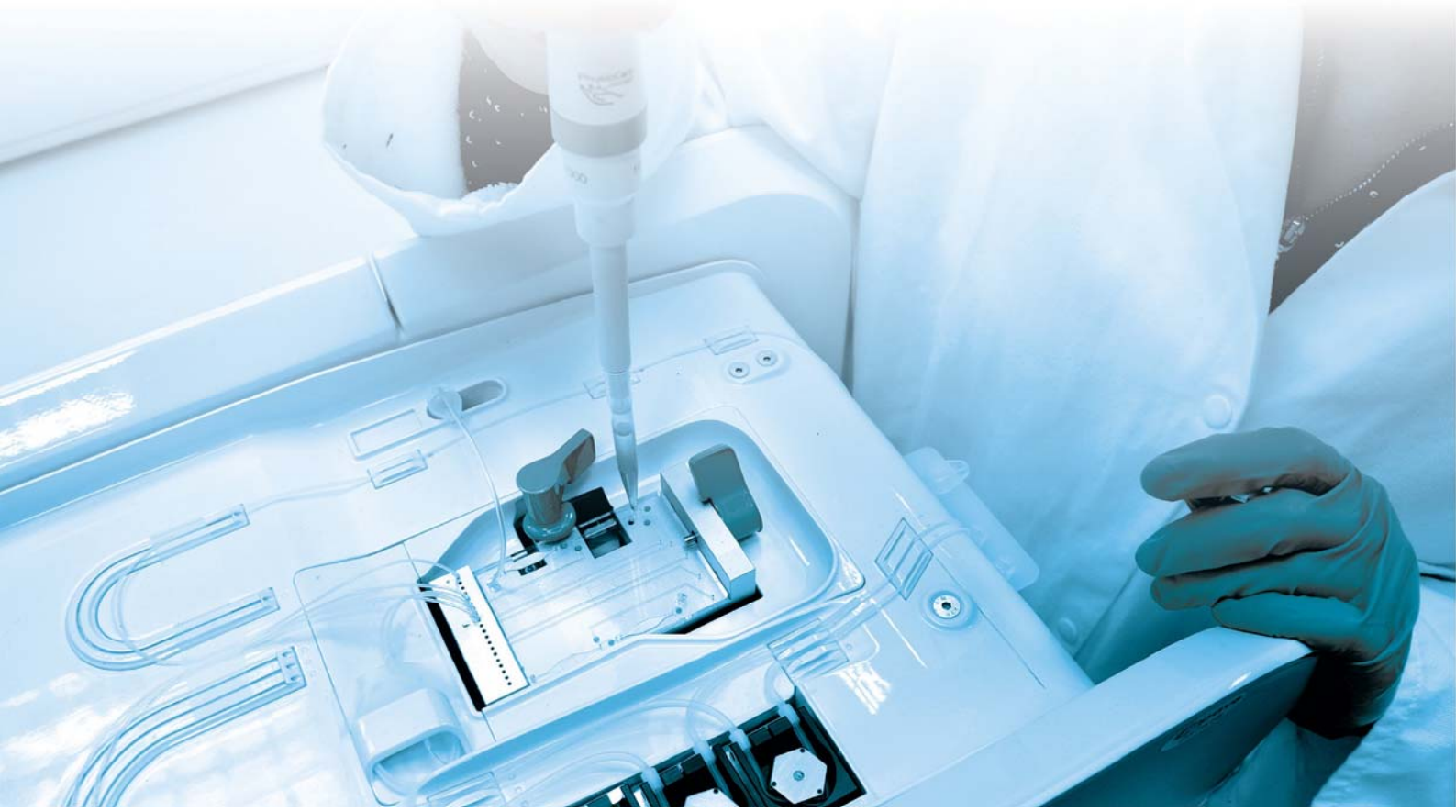

6

NANOTECHNOLOGIES

- Lipid nanoparticules
- Nanocharacterization
- Drug vectorization
- Nanotherapeutics
- Electrochemistry sensor

Development of characterization methods for Lipidot® multifunctional platform: a step forward industrial transfer

Lipid nanoparticles, Nanomedicine, Nanocharacterization, Standardization

Authors: M. Varache, M. Ciancone, F. Caputo, C. Laffont, M. Escudé, E. Rustique, D. Jary, P. Boisseau, I. Texier, F. Navarro, A.-C. Couffin

Abstract: Lipidot® Platform has evolved towards the design of innovative matrices combining lipid nanoparticles for proteins/biomacromolecules delivery and eventually polymeric materials thanks to European and industrial projects. At this stage of development, characterization of nanotherapeutics is a key parameter to ensure quality of final products. We are seeking to implement a panel of methods of characterization significantly suitable for nanoparticles. More particularly, we have investigated the lipid quantification, the drug/protein encapsulation, release kinetics and leakage to understand/anticipate the behavior of matrices in biological media and in various applications related to healthcare.

Context and Challenges

Over last 3 years, Lipidot® technology has thrived towards a versatile nanodelivery platform for designing and producing a series of nanoproducts for *in vitro* diagnostic, *in vivo* imaging, activated or non-activated targeted drug delivery [1, 2].
Nanotherapeutics are classified as therapeutics by all major medicine regulation agencies claiming a qualification according to the existing rules and regulations for pharmaceutical or medical device development. However, standards are sometimes missing in areas such as analytical or physical-chemical methods related to nanoscale features. A more deep understanding of nanoparticles composition, morphology, aggregation, crystallinity as well as nanoparticles interaction with proteins in biological fluids is crucial to meet the requirements of final medicinal nanoproducts.

Main Results

Complementary physical chemical charac-terization methods have been used to determine the morphology, the size, the shape and the surface charge of the Lipidots®. For example, the internal physical state of the particle core has been studied by Differential Scanning Calorimetry (DSC), ^{1}H NMR spectroscopy, and Small-Angle Neutron Scattering (SANS). Localization of different encapsulated drugs within the nanodroplets has been characterized by NMR spectroscopy and correlated with the loading profiles (Figure 1).

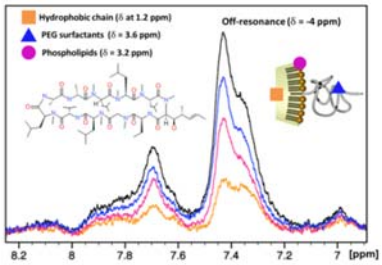

Figure 1: Drug Localization into Lipidots® performed by ^{1}H NMR NOEDIFF spectroscopy. Example of cyclosporine loaded into 50 nm-size droplets located at once in the core and the shell of nanoparticles.

The quantification and identification of Lipidot® components (e.g. mixture of mono-, di-, and triglycerides, phospholipids and PEGylated surfactants) have been performed by using validated H/UPLC-ELSD methods and mass spectrometry detection (Figure 2). A "fingerprint approach" was established for Lipidot® nanoparticles based on lipid composition and content, enabling to follow up any evolution during manufacturing process and ageing of formulations. In order to predict the *in vivo* behavior of the nano-therapeutics, we developed a suitable and transposable tool for separation and quantification of free and entrapped drugs/dyes by combining Solid Phase Extraction and Drug Content Determination (DCD) [3]. Such methods allow studying drug leakage kinetics under storage conditions and the drug release profiles in different biological media. HPLC quantification combined with spectroscopic techniques has been also routinely performed for optimization of payload formulation.

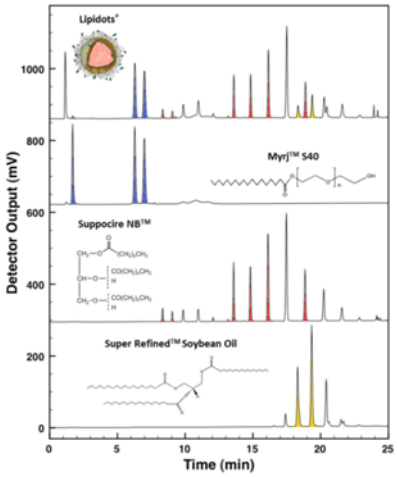

Figure 2: Quantification of Lipidots components. Chromatograms of Lipidot® and individual lipid excipients assessed by UPLC-ELSD for 50 nm-size formulation.

Perspectives

Extensive characterization dedicated specifically to Lipidot® as a nanomedicine allows identifying characterization criteria and specifications to move towards industrial production and approval of the product for the clinical market. Very recently our group has also begun to coordinate the European Nanomedicine Characterization laboratory. Connected to a trans-disciplinary testing infrastructure, this platform will propose a cascade of assays for the pre-clinical characterization of nanoparticles, promoting the translation of nano-products towards clinical evaluation faster and for lower cost and also paving the way for future pre-normative activities in order to regulate the development of nanomedicines.

Related Publications:
[1] T. Delmas and al., "Preparation and characterization of highly stable lipid nanoparticles with amorphous core of tuneable viscosity", Journal of Colloid and Interface Science 2011, 360, 471–481.
[2] F. Navarro, G. Creusat, C. Frochot, A. Moussaron, M. Verhille, R. Vanderesse, J.-S. Thomann, P., I. Texier, A.-C. Couffin, M. Barberi-Heyob, "Preparation and characterization of mTHPC-loaded solid lipid nanoparticles for photodynamic therapy", Journal of Photochemistry and Photobiology B: Biology, 2014,130, 161–169.
[3] A. Guillot, A.-C. Couffin, X. Sejean, F. Navarro, M. Limberger, C.-M. Lehr, "Solid Phase Extraction as an Innovative Separation Method for Measuring Free and Entrapped Drug in Lipid Nanoparticles", Pharmaceutical Research, 2015 32(12): 3999-4009.

Comparative biodistribution in mice of cyanine dyes loaded in lipid nanoparticles

Research topic: Drug vectorization, Lipid nanoparticles, Fluorescent contrast agent

Authors: J. Mérian, I. Texier

Abstract: The biodistribution of two cyanine dyes, ICG and DiD, when loaded in solid lipid nanoparticles (LNP) were compared to that of a radiolabeled lipid included in the nanoparticle core. Whereas LNP-DiD and LNP-ICG presented the same features in aqueous buffer (physico-chemical characteristics and stability of the particles), ICG leaked out of the particles as soon as injected in mouse blood resulting in renal elimination of the dye, whereas DiD and the lipid tracer circulated in blood before being metabolized in the liver. This difference of pattern is accounted for by the high affinity of ICG for plasma proteins, driving the leakage of the dye.

Context and Challenges

Nanoparticles are expected to overcome many challenges in the delivery of drugs in future years [1]. Their main interest lies in their potential to achieve better vectorization of the active ingredients that they encapsulate or that are attached to their surface, to the biological targets. A technology of solid lipid nanoparticles (LNP) with viscous non-crystalline lipid core dedicated to drug vectorization has been developed using a solvent-free sonication process, using FDA approved ingredients, for several years in the department (Lipidots™ technology) [2, 3]. However, the fate of the loaded drug after *in vivo* injection cannot always be predicted based on the usually investigated physico-chemical characteristics of the drug-loaded particles. This is demonstrated in the present study in which the biodistribution of two cyanine dyes, with very close chemical structures, ICG and DiD, when loaded in solid lipid nanoparticles (LNP), were compared to that of a radiolabeled lipid included in the nanoparticle core [4].

Main Results

Two near infrared cyanine dyes, DiD (1,1'-dioctadecyl-3,3,3',3'-tetramethylindotricarbocyanine perchlorate) and ICG (Indocyanine Green) were loaded in lipid nanoparticles (LNP). DiD-LNP and ICG-LNP presented similar physicochemical characteristics (hydrodynamic diameter, polydispersity, zeta potential), encapsulation efficiency, and colloidal stability when stored in PBS buffer.

However, whereas DiD had similar biodistribution than cholesteryl-1-^{14}C-oleate ([^{14}C]CHO, a constituent of the nanoparticle used as a reference radiotracer), ICG displayed a different biodistribution pattern, similar to that of the free dye, indicative of its immediate leakage from the nanovector after blood injection (Figure 1).

NMR spectroscopy using Proton NOE (Nuclear Overhauser Effect) measurements showed that the localization of the dye in the lipid nanoparticles was slightly different: ICG, more amphiphilic than DiD, was found both inside the lipid core and at particle interface, whereas DiD, more hydrophobic, appeared exclusively located inside the particle core.

The ICG release rate from the particles was 7% per 1 month under storage conditions (4°C, dark, 10% of lipids), whereas no leakage could be detected for DiD. ICG leakage increased considerably in the presence of Bovine Serum Albumin 40 g/L (45% leakage in 24 h at 100 mg/mL of lipids), because of the high affinity of the fluorophore for plasma proteins. On the contrary, no DiD leakage was observed, until high dilution of the nanoparticles which triggered their dissociation (45% leakage in 24 h at 1 mg/mL of lipids). Altogether, the subtle difference in dye localization into the nanoparticles, the partial dissociation of the LNP in diluted media, and more importantly the high ICG affinity for plasma proteins, accounted for the differences observed in the fluorescence biodistribution after tail vein injection of the dye-loaded nanoparticles.

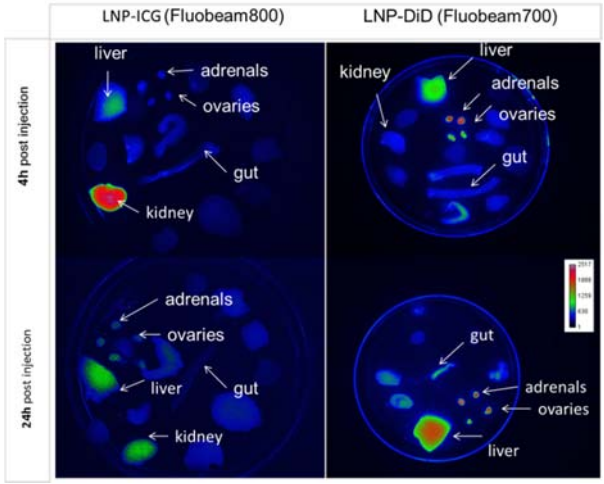

Figure 1: Fluorescence images of resected organs obtained 4 h and 24 h after tail vein injection of ICG-LNP-14C and DiD-LNP-14C particles.

Perspectives

These results highlight the large impact that subtle differences in drug structure can have on their biodistribution after *in vivo* injection, even when using the same nanoparticle as vehicle. Going through high level characterization (such as NOE for the drug fine localization into the particle structure) and *in vitro* thorough biological studies are therefore necessary in order to gain in predictability of the behavior of drug-loaded nanosystems when injected in blood.

Related Publications:
[1] A. Hafner, J. Lovric, G. Lakos, I. Pepic, "Nanotherapeutics in the EU: an overview on current state and future directions", Int. J. Nanomed. 9 (2014) 1005-1023.
[2] T. Delmas, A.-C. Couffin, P.-A. Bayle, F. d. Crécy, E. Neumann, F. Vinet, M. Bardet, J. Bibette, I. Texier, "Preparation and characterisation of highly stable lipid nanoparticles with amorphous core of tuneable viscosity", J. Colloid Interf. Sci. 360 (2011) 471-481.
[3] T. Delmas, H. Piraux, A.-C. Couffin, I. Texier, F. Vinet, P. Poulin, M. E. Cates, J. Bibette, "How to prepare and stabilize very small nanoemulsions", Langmuir 27 (2011) 1683-1692.
[4] J. Mérian, R. Boisgard, P.-A. Bayle, M. Bardet, B. Tavitian, I. Texier, "Comparative biodistribution in mice of cyanine dyes loaded in lipid nanoparticles", Eur. J. Pharm. Biopharm. 93 (2015), 1-10.

First *in vitro* characterization of novel nucleic acid-based nanocomplexes for the treatment of antibiotic resistant pathogens

Research topic: Nanotherapeutics for antibiotic resistant emerging bacterial pathogens

Authors: A. Hibbitts, M. Menneteau, D. Jary, F. Navarro

Abstract: Transcription factor decoys (TFDs) were complexed with cationic lipid nanoparticles (cLNPS) for cellular delivery and enhanced stability. TFD-cLNP nanocomplexes were analyzed for size, zeta potential and electrophoretic mobility following incubation in a range of biologically relevant media. Nanocomplexes were also titrated over a pH gradient and the behavior recorded. Following this, nanocomplex toxicity in THP-1 macrophage cells was assessed using WST-1 assays over a range of TFD and cLNP concentrations. TFD-cLNPs were found to be stable up to 24 hrs+ depending on the media and were well tolerated in THP-1 cells in a dose dependent manner.

Context and Challenges

TFDs represent a new means of overcoming bacterial resistance [1, 2]. TFDs function by binding transcription factor proteins in place of their intended DNA strands, thereby resulting in transcription inhibition. Since one transcription factor can potentially modulate several different genes, there is a great potential for TFDs to successfully inhibit bacterial growth without the need for antibiotics.

However, as with all nucleic acid based therapies, efficient and safe delivery of the TFD remains a key factor. Specifically, there are the difficulties in reaching either intracellular pathogens or traversing gram positive bacterial cell wells. In this study, we attempted to address this by complexing TFDs with the novel cLNPs we have developed [3]. Suitability for continued study was assessed via *in vitro* stability assays and *in vitro* cell viability.

Main Results

- *In vitro* Stability of cLNP-TFD Nanocomplexes in Biologically Relevant Media

Nanocomplex size remained stable for a minimum of 24 hrs in all cases. In PBS (Figure 1A), RPMI media + 25 mM HEPES (Figure 1B), LB broth and RPMI media + 10% FBS.

A.

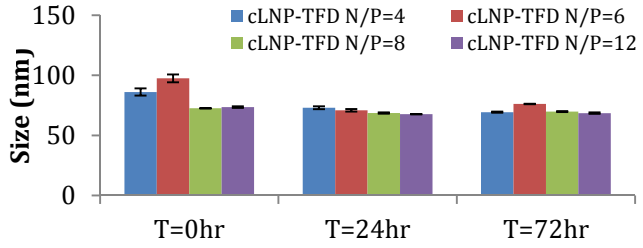

B.

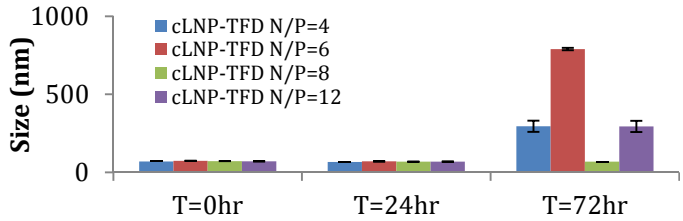

Figure 1: Size analysis of cLNP-TFD nanocomplexes over 72hrs in A) PBS and B) RPMI media + 25mM HEPES buffer.

- THP-1 Cell Viability Studies using cLNP-TFD Nanocomplexes

To determine the operating range of cLNP-TFD nanocomplexes, a series of cell viability tests were undertaken. At 20 nM TFD, only cLNP nanocomplexes were found to be well tolerated up to N/P=100 (Figure 2). Other viability studies found that at 100 nM TFD, decreases in viability of up to 40% were observed.

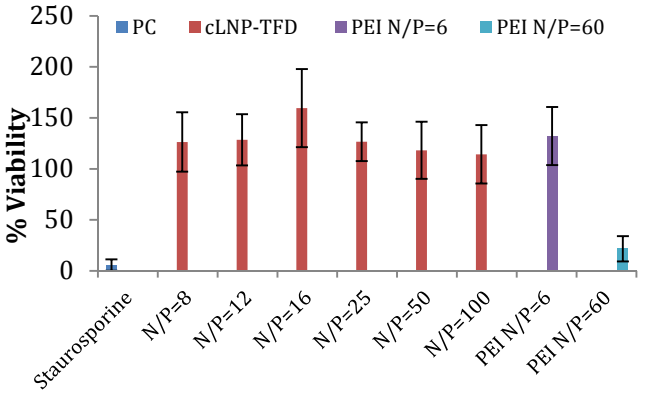

Figure 2: WST-1 cell viability assay on THP-1 cells transfected with cLNP-TFD or PEI-TFD at 20nM concentration (n=3 ±SD).

This work is part of the NAREB European research network supported by the EU FP7 under grant agreement 604237. TFDs were synthesised and supplied by Procarta Biosystems/ University of East Anglia as part of the NAREB research consortium.

Perspectives

From these studies, cLNP-TFD nanocomplexes displayed high levels of stability across a range of environments. Nanocomplexes were also well tolerated at high doses. These results now allow for future in-depth cellular and microbiological screening.

Related Publications:
[1] "Global tuberculosis control: surveillance, planning, financing", WHO report 2012.
[2] Tiemersma and al., Emerg Infect Dis. 2004;10:1627–1634.
[3] T. Delmas, A.-C. Couffin, P.-A. Bayle, F. de Crécy, E. Neumann, F. Vinet, M. Bardet, J. Bibette, I. Texier, "Preparation and characterization of highly stable lipid nanoparticles with amorphous core of tuneable viscosity", J Colloid Interface Sci. 2011 Aug 15;360(2):471-81.
[4] A Hibbitts, M. Menneteau, D. Jary, F. Navarro, "First *In Vitro* Characterization of Novel Nucleic Acid-Based Nanocomplexes for the Treatment of Antibiotic Resistant Pathogens", 2015, 2015 CRS Annual 2°15 Meeting, July 26-29 Edinburgh,Scotland.

Electrochemistry provides a simple way to monitor pseudomonas aeruginosa metabolites

Research topic: Electrochemistry for bacteria monitoring

Authors: J. Oziat, P. Mailley

Abstract: *Pseudomonas aeruginosa* is one of the most common bacteria responsible for nosocomial infections. To imagine new therapies, understanding virulence mechanisms and the associated communication system of the bacterium is a target of the first importance. Electrochemistry is a promising tool for real-time *in-situ* monitoring of electroactive species issued from bacteria communication system. Here *P. aeruginosa* metabolites, Pseudomonas Quinolone Signal and pyocyanin, were electrochemically characterized and further detected in supernatant of *P. aeruginosa* PA01 strain grown in LB medium.

Context and Challenges

Pseudomonas aeruginosa (PA), a gram-negative, ubiquitous and naturally multi-resistant bacterium, is the fourth most common bacteria responsible for nosocomial infections in Europe [1]. To better study this bacterium and its impact, most of the research has focused on its communication system, usually referred to as the quorum sensing (QS). Today, three interconnected QS systems are known. The standard method to study these metabolites is through liquid chromatography–mass spectrometry (LC/MS). This method leads to quantitatively reliable results but requires the extraction of supernatant from the growth medium and expansive instrumentation. Recently, researchers became interested in methods that allow quick *in-situ* analyses as electrochemistry.

Main Results

The electrochemical behaviors of three PA metabolites (Pseudomonas Quinolone Signal (PQS) and pyocyanin (PYO)) were explored by cyclic voltammetry in PBS with a glassy-carbon (GC) working-electrode (see Figure 1) [2]. As reported by several teams, PYO is a quasi-reversible and highly-responsive species that undergoes electrochemical reaction around -0.25 V in PBS. PQS voltammetric signal are markedly less intense and less reversible than PYO. Clear oxidation and reduction peaks are seen near 0.18 V. The lower current may be associated to the lipophilic PQS alkane tail that implies either slower diffusion in the electrolyte or adsorption on the electrode thus blocking electron exchanges.

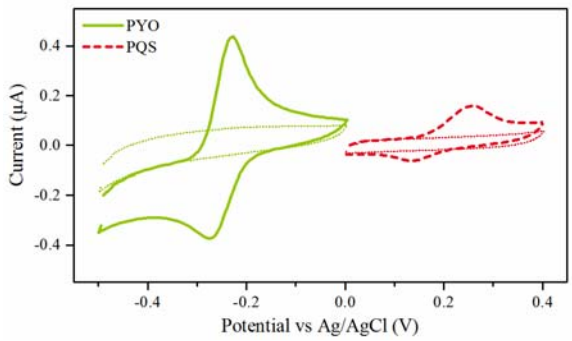

Figure 1: Cyclic voltammetry of PQS, PYO and 2'-AA 100 µM in PBS on GC electrode.

To validate the use of QS electrochemistry as a tool for bacteria monitoring, we performed the detection of PYO and PQS in real culture medium [2]. To do so, filtrated supernatant of PA01 culture was electrochemically analyzed on GC electrode (square wave voltammetry on the potential range of -0.6/+0.6 V). On this potential range, seven different peaks with variable intensity are visible (see Figure 2) from which one can distinguish PYO and PQS responses at -0.25 and +0.18 V vs Ag/AgCl, respectively. The thin 0.25 V peak of PYO became visible after 4h of growth and increase until 24h of growth. Interestingly, one can notice the cathodic shift of the PYO peak over culture time due to alkalization of the medium as already reported for PA. PQS is seen near 0.17 V in a short time window: the peak increases from 6 to 8h before falling down at 24h. These results are very consistent with literature ones, showing a PQS maximum at the beginning of the stationary phase, before concentration fell down during the second part of the stationary phase. The presence of several other peaks confirmed the production of other electrochemically active species by PA. Literature data cannot lead to clearly identification of these species but they may belong at quinolones or phenazines families.

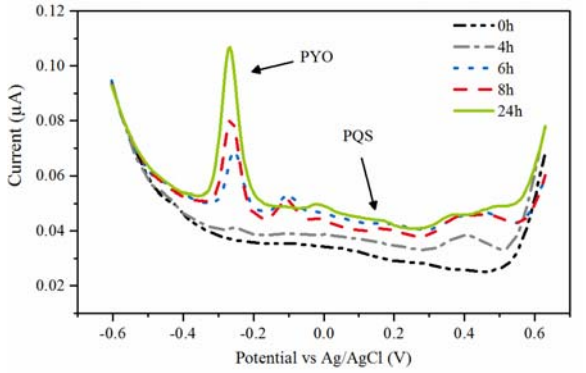

Figure 2: Square wave voltammetry of PAO1 supernatant on GC electrode.

Perspectives

Next work concerns improvement of the detection limit through utilization of the conducting polymer PEDOT:PSS. A huge staking between the metabolites and the organic ring of the polymer should enhance the signal.

Related Publications:
[1] European Centre for Disease Prevention and Control, "Surveillance report - Point prevalence survey of healthcare-associated infections and antimicrobial use in European long-term care facilities", 2013.
[2] J. Oziat, S. Elsen, R. M. Owens, G. G. Malliaras, P. Mailley, "Electrochemistry provides a simple way to monitor Pseudomonas aeruginosa metabolites", Proceeding of Engineering in Medicine and Biology Society (EMBC), 37th Annual International Conference of the IEEE, 2015.

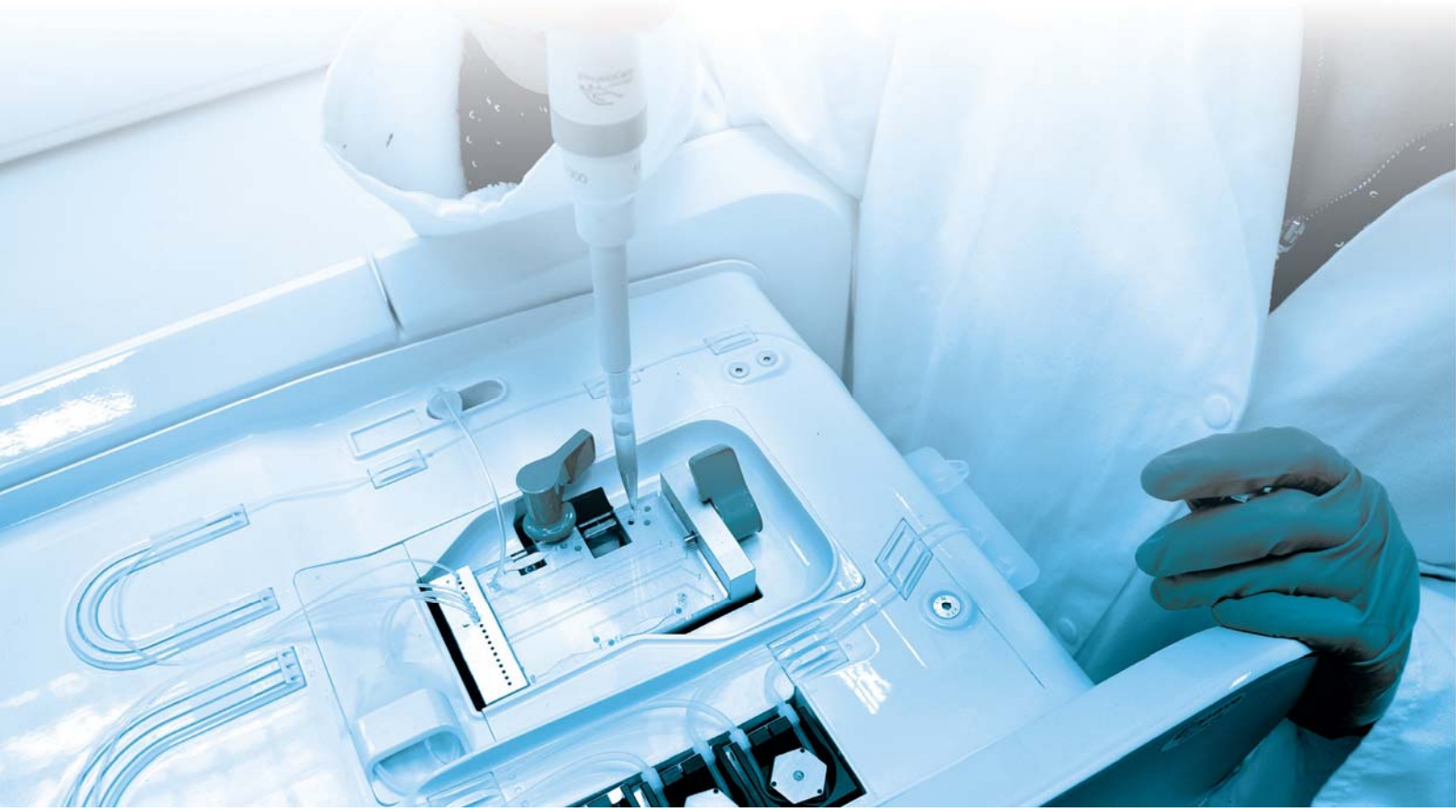

7

PHD DEGREE AWARDED

- Blandine Roig
- Julien El Sabahy
- Florian Pineda
- Alexandre Fouchard
- Raphaëlle Roy
- Marjorie Vrignaud

Blandine Roig

University Reims-Champagne-Ardenne, France

CUTANEOUS TISSUE CHARACTERIZATION WITH BIMODAL SPECTROSCOPY: DIFFUSE REFLECTANCE AND RAMAN

This thesis relates to the combination of two *in vivo* skin characterization techniques. On the one hand, Diffuse Reflectance Spectroscopy (DRS) enables skin optical properties characterization by quantifying light absorption and light elastic scattering. On the other hand, Raman microspectroscopy provides information on molecular compositions of tissues with no need of labeling. Localization and quantification functions of Raman microspectroscopy are both distorted in scattering media such as skin. Therefore, the aim of this thesis was to assess the effect of light-matter interactions on these functions. A bimodal method is proposed to achieve quantitative biochemical characterization of cutaneous tissues *in vivo*. The main idea is to develop a procedure of Raman spectra correction based on the quantified optical properties provided by DRS. This work was divided in three complementary approaches: the development of a system enabling diffuse reflectance and optical properties measurements in the same zone as Raman microspectroscopy; the fabrication of optical phantoms improving our knowledge on absorption, elastic scattering and Raman scattering phenomena; and the development of a Raman spectra correction model as function of the skin optical properties given by DRS measurements.

Julien El Sabahy

University Grenoble Alpes, France

PECVD ORGANOSILICATE THIN FILMS FOR GAS SENSOR FUNCTIONALIZATION

Gas detection is a growing field, both for indoor and outdoor air quality monitoring and for process monitoring. It is indeed particularly critical in the case of volatile organic compounds (VOC) whose impact on public health is proven. Detecting and quantifying their presence becomes a major problem and various solutions are available. One of them, based on the coupling of a resonant beam and a chromatography micro column, appears to be a promising solution. Those two devices combine selectivity and high sensitivity; however, they require functionalization with a sensitive layer.

This work focused on SiOCH thin films deposited by PECVD. The gas interaction of the sensitive layers deposited during this work was studied using quartz crystal microbalances (QCM). The obtained measurements were then correlated to a simple model, providing an interpretation of the interaction – for steady-state but also kinetic regime - between the SiOCH and the gas of interest.

The first part of the study shows the impact of the chemical composition of those materials on their affinity for toluene, representative for aromatic VOCs. Relying on physico-chemical characterization techniques, the role of various chemical bonds on the solid/gas interaction was investigated. This work shows that a compromise between chemical composition and hydrophobicity has to be reached to preserve SiOCH affinity and temporal response.

The influence of porosity was then explored in a second step to further increase the sensitivity of those materials. Original deposition processes were developed in order to propose new porous materials with higher toluene affinity. The limits of the subtractive approach generally used for these PECVD materials (i.e. the porogen approach) were then overcome in terms of porosity and pore size. Concerning gas detection, it is difficult to decorrelate between the impact of chemistry and porosity. Whatever, increasing porosity does not appear to be the only relevant parameter in order to increase these materials affinity at low concentrations.

Florian Pineda

Grenoble INP - Phelma / University Grenoble Alpes, France

FLEXIBLE AND STRETCHABLE MICROFLUIDICS

Mechanical properties of hyper elastic elastomers provide new opportunities to captors, radio frequencies antennas and soft robots. This work is focused on the study of a hyper elastic material called Ecoflex and on its integration in microfluidic systems using its exceptional mechanical properties.

First, material's mechanical properties were investigated during membrane blowing experiments. Simulations based on the phenomenological model of Mooney-Rivlin were developed and validated. These results were useful to the development of two applications.

First application of hyper elastic system is an elongation sensor. Electro fluidic sensors combine Ecoflex's hyper elastic properties and Galinstan's electrical properties. Galinstan is a metallic alloy which is liquid at room temperature. A microchannel molded in the elastomer and filled with the liquid metal form an electrical resistance. Sensor's deformation induces a geometrical change into the channel and therefore a variation of the electrical resistance. Characterization tests performed on these sensors showed capabilities to measure large elongations and reversibly without loss of electrical contact. An elongation of the sensor's length by a factor 4 involves an increase of the electrical resistance by a factor 8 providing a good sensibility of the system. Results according to the sensor's geometry are discussed using simulation tools, analytical study and experimental data.

Second application is the development of hyper elastic reservoirs integrated into microfluidic cards. Inspired from membrane blowing tests, they are able to store volumes from few microliters to milliliters of reagents without taking too much place on the microfluidic cards' surface. Membranes' elasticity naturally pressurizes the reservoir when it is filled and a simple optical edge detection method gives the internal volume in real time. Combined with pneumatic valves these reservoirs inject precise volumes into a microfluidic network. Different microfluidic systems were developed, a simple reservoir with two valves for the characterizations and cards with multiple reservoirs to realize complex protocols like on demand dilution or automated ELISA test.

Alexandre Fouchard

University Grenoble Alpes, France

ELECTRICAL IMPEDANCE TOMOGRAPHY WITH MULTICONTACT CUFF MICROELECTRODES: TOWARDS PERIPHERAL NERVE IMAGING

Medical electrical stimulators adapted to peripheral nerves make use of multicontact cuff electrodes (MCC). Intended until now for stimulation or recording, MCC can also be used as a means of transduction to characterize the nerve by impedancemetry. The objective of this thesis is to determine the feasibility of obtaining information on the electrical property distribution of a nerve section, through electrical impedance tomography (EIT) using microelectrode arrays.

A transversal approach is put forward to address this question. It encompasses methodological developments in electrical imaging and their *in vivo* application in rodents. The literature review on the EIT principle and its applications in neuroimaging identified two means of mapping the electrical properties of a nerve: (i) multifrequency structural imaging, (ii) functional imaging of the impedance variation occurring during action potential propagation.

The design and implementation of an experimental device allowed understanding the signal properties and the source of contrast in EIT. The following voltage data prediction (forward problem) relied on a generic finite element library, or on a mixed finite element - finite volume method (FVE). Parameter estimation (inverse problem) was handled by transport methods, and by multifrequency approaches using a constrained optimization. *In vivo* experiments showed recordings of compound action potentials (CAP), and revealed associated impedance variations.

Prospects include upgrading the *in vivo* EIT system and integrating new multicontact devices, to record a spatially-localized impedance variation. Eventually, regions that are interesting to be targeted by stimulation could be identified through this means.

Raphaëlle Roy

University Grenoble Alpes, France

STUDY OF ELECTROPHYSIOLOGICAL CORRELATES FOR THE DISCRIMINATION OF MENTAL FATIGUE AND WORKLOAD STATE MONITORING: CONTRIBUTION TO PASSIVE BRAIN-COMPUTER INTERFACES

Mental state estimation on the basis of cerebral activity and its resulting physiological activities has become a challenge for passive Brain-Computer Interfaces (BCI), in particular to address a need in neuroergonomics. This thesis work focuses on mental fatigue and workload estimation. Its purpose is to provide efficient and realistic processing chains. Thus, one issue was the modulation of workload markers as well as classification performance robustness depending on time-on-task (TOT). The impact of workload and TOT on attentional state markers was also assessed. For those purposes, an experimental protocol was implemented to collect the electroencephalographic (EEG), cardiac (ECG) and ocular (EOG) signals from healthy volunteers as they performed for a prolonged period of time a task that mixes working memory load and selective attention. Efficient signal processing chains that include spatial filtering and classification steps were designed in order to better estimate these mental states. The relevance of several electrophysiological markers was compared, among which spontaneous EEG activity and event-related potentials (ERPs), as well as various preprocessing steps such as spatial filtering methods for ERPs. Interaction effects between mental states were brought to light. In particular, TOT negatively impacted mental workload estimation when using power features. However, the chain based on ERPs was robust to this effect. A comparison of the type of stimuli that can be used to elicit the ERPs revealed that task-independent probes still allow very high performance, which shows their relevance for real-life implementation. Lastly, ongoing work that aims at assessing task-robust workload markers, as well as the usefulness of auditory ERPs in a single-stimulus paradigm will be presented as prospects.

Marjorie Vrignaud

University Grenoble Alpes, France

NANOPOROUS MATERIALS FOR THE OPTICAL DETECTION OF MICROBIAL VOLATILE ORGANIC COMPOUNDS

The presence of micro-organisms can be revealed by specific volatile metabolites. This approach is interesting for the non-invasive detection of pathogenic species in complex samples, such as food, blood or exudate. Nanoporous materials developing a high surface area have been prepared by sol-gel process (xerogels). They trap, concentrate and reveal the presence of microbial Volatile Organic Compounds (VOC) by means of an optical detection. Sensors have been doped with a probe molecule (5,5′ -dithiobis 2-nitrobenzoic acid) in order to detect hydrogen sulfide emitted by foodborne pathogen Salmonella. The colour of sensor changes in the presence of 5 ppm of H2S.

Another detection method is the use of enzymatic substrates which release exogenous VOCs. In this approach, the enzymatic activity is specific to the targeted pathogenic bacteria. Sensors have been developed for two exogenous VOCs: β-naphthylamine (β-NA) and 2-nitrophenol (2-NP). β-NA is issued from peptidase activity, whereas 2-NP is produced by glycosidase or esterase activity. The latter can be detected above 14 ppb through absorbance in the visible region. The work focused both on the chemical composition of the xerogels and on their shape. After molding the xerogels into a trihedral prism (“corner reflector”), the absorbance can be easily monitored using the reflected light. VOCs produced by 3 pathogenic bacteria, Salmonella, Escherichia coli and Staphylococcus aureus, in complex media (blood and food samples) have been monitored with the obtained sensors.

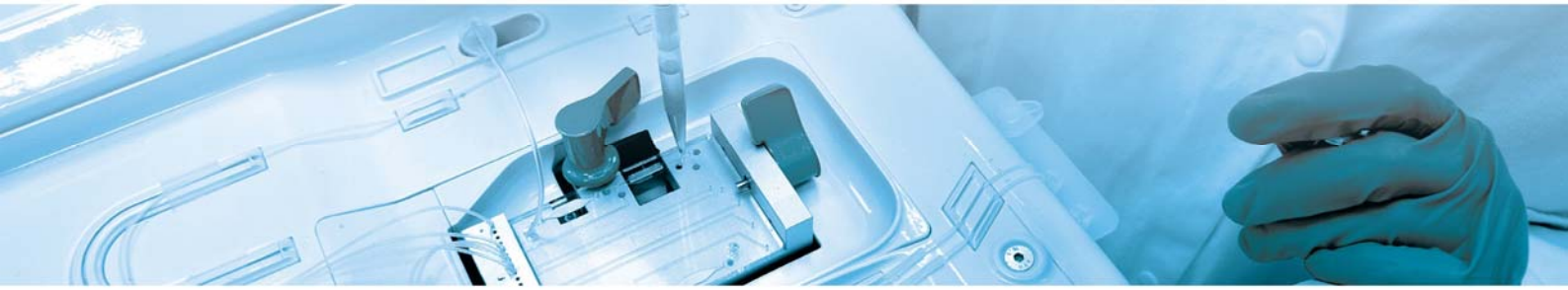

Greetings

EDITORIAL COMMITTEE
Béatrice Icard
Fabrice Navarro
Séverine Vignoud
Pascal Mailley
Jean-Marc Dinten
Loïck Verger
Pierre Jallon
Régis Guillemaud
Hélène Vatouyas
Sandra Barbier
Pierre Grangeat
Abdelmadjid Hihi

GRAPHIC DESIGN
Eve Issartel, DesignbyEve
Hélène Vatouyas

SPECIAL THANKS
Bénédicte Messina

PHOTOS

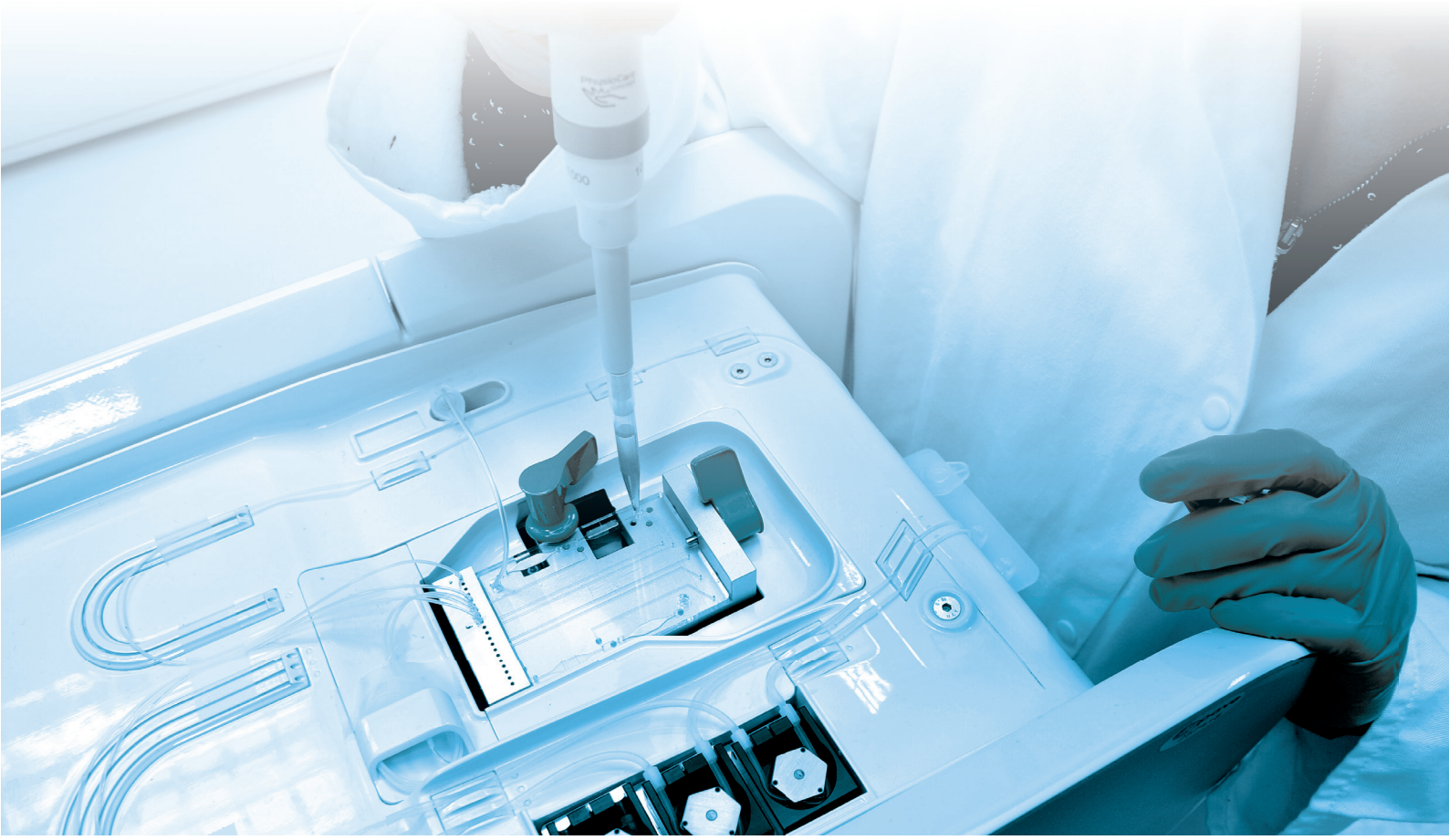

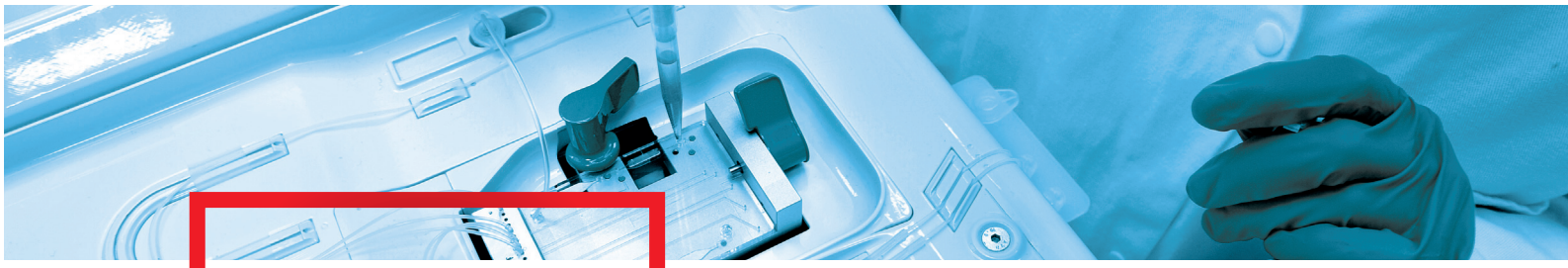

TECHNOLOGIES FOR BIOLOGY AND HEALTH

Contacts

Daniel Vellou
Head of Microtechnologies for Biology and Healthcare division
daniel.vellou@cea.fr

Régis Guillemaud
Chief Scientist
regis.guillemaud@cea.fr

Patrick Boisseau
Business development - nanomedicine
patrick.boisseau@cea.fr

Olivier Fuchs
Business development - implantable medical device, agriculture, food
olivier.fuchs@cea.fr

Anca-Nicoleta Galatanu
Business development - X-ray and gamma ray for NDT & security
anca-nicoleta.galatanu@cea.fr

Francis Glasser
Business development - medical imaging
francis.glasser@cea.fr

Eric Gouze
Business development - medical device & connected health
eric.gouze@cea.fr

Gilles Marchand
Business development - chemistry, cosmetics, pharmacy, environment & process monitoring
gilles.marchand@cea.fr

Alexandre Thermet
Business development - in vitro diagnostic & vaccine
alexandre.thermet@cea.fr

Jean-Claude Royer
Clinatec Director of Operations
jean-claude.royer@cea.fr

Peggy Rematier
Clinatec industrial alliances Manager
peggy.rematier@cea.fr

Abdelmadjid Hihi
Clinatec Scientific program Manager
abdelmadjid.hihi@cea.fr

Leti, technology research institute
Commissariat à l'énergie atomique et aux énergies alternatives
Minatec Campus | 17 rue des Martyrs | 38054 Grenoble Cedex 9 | France
www.leti.fr